**Atmospheric
Chemistry
and Physics**

Isoprene oxidation mechanisms: measurements and modelling of OH and HO$_2$ over a South-East Asian tropical rainforest during the OP3 field campaign

D. Stone[1,2], M. J. Evans[1], P. M. Edwards[2], R. Commane[2,*], T. Ingham[2,3], A. R. Rickard[2,3], D. M. Brookes[4],
J. Hopkins[5,6], R. J. Leigh[4], A. C. Lewis[5,6], P. S. Monks[4], D. Oram[7,8], C. E. Reeves[7,8], D. Stewart[7,**], and D. E. Heard[2,3]

[1]School of Earth & Environment, University of Leeds, Leeds, UK
[2]School of Chemistry, University of Leeds, Leeds, UK
[3]National Centre for Atmospheric Science, University of Leeds, Leeds, UK
[4]Department of Chemistry, University of Leicester, Leicester, UK
[5]Department of Chemistry, University of York, York, UK
[6]National Centre for Atmospheric Science, University of York, York, UK
[7]School of Environmental Sciences, University of East Anglia, Norwich, UK
[8]National Centre for Atmospheric Science, University of East Anglia, Norwich, UK
*now at: School of Engineering & Applied Sciences, Harvard University, Cambridge, USA
**now at: Department of Chemistry, University of Reading, Reading, UK

Abstract. Forests are the dominant source of volatile organic compounds into the atmosphere, with isoprene being the most significant species. The oxidation chemistry of these compounds is a significant driver of local, regional and global atmospheric composition. Observations made over Borneo during the OP3 project in 2008, together with an observationally constrained box model are used to assess our understanding of this oxidation chemistry. In line with previous work in tropical forests, we find that the standard model based on MCM chemistry significantly underestimates the observed OH concentrations. Geometric mean observed to modelled ratios of OH and HO$_2$ in airmasses impacted with isoprene are $5.32^{+3.68}_{-4.43}$ and $1.18^{+0.30}_{-0.30}$ respectively, with 68 % of the observations being within the specified variation. We implement a variety of mechanistic changes into the model, including epoxide formation and unimolecular decomposition of isoprene peroxy radicals, and assess their impact on the model success. We conclude that none of the current suggestions can simultaneously remove the bias from both OH and HO$_2$ simulations and believe that detailed laboratory studies are now needed to resolve this issue.

1 Introduction

Atmospheric oxidation, predominantly initiated by the hydroxyl radical (OH), removes biogenically and anthropogenically emitted volatile organic compounds (VOCs) from the atmosphere. The reaction of OH with VOCs leads to a complex cascade of reactions and species. Understanding this cascade is a significant challenge for atmospheric chemistry and climate. Isoprene (C$_5$H$_8$) is produced by the biosphere and is the dominant biogenic VOC emitted into the atmosphere. A good representation of its chemistry is central to our ability to understand the past, present and future composition of the atmosphere.

Previous studies have suggested significant flaws in our ability to understand isoprene oxidation chemistry, notably through a significant underestimate of the OH concentration in air with low concentrations of nitrogen oxides but high concentrations of isoprene (Carslaw et al., 2001; Tan et al., 2001; Thornton et al., 2002; Ren et al., 2008; Butler et al., 2008; Kubistin et al., 2010; Lelieveld et al., 2008; Martinez et al., 2010; Hofzumahaus et al., 2009; Pugh et al., 2010; Wolfe et al., 2011; Whalley et al., 2011). Field studies, chamber studies and theoretical chemical studies have all recently investigated the oxidation of isoprene under low NO$_x$ conditions.

Studies of OH and HO_2 chemistry in a forested region of Greece during the AEROBIC97 (Aerosol formation from Biogenic organic Carbon 1997) campaign (Carslaw et al., 2001) and in isoprene-rich regions during the INTEX-A (Intercontinental Chemical Transport Experiment-A) (Ren et al., 2008) noted significant model underpredictions of OH concentrations but failed to offer any mechanistic explanations.

During the Guyanas Atmosphere-Biosphere exchange and Radicals Intensive Experiment with the Learjet (GABRIEL) campaign, OH and HO_2 observations were made over the Amazonian rainforest (Lelieveld et al., 2008; Martinez et al., 2010). Model simulations with both the ECHAM5/MESSy global chemistry-climate model (Butler et al., 2008; Lelieveld et al., 2008) and the MECCA box model (Kubistin et al., 2010; Lelieveld et al., 2008), using chemistry derived from the Master Chemical Mechanism (MCM) (Jenkin et al., 2003; Saunders et al., 2003), significantly underestimated the observed HO_x concentrations, with mean observed to modelled ratios of 12.2 ± 3.5 for OH and 4.1 ± 1.4 for HO_2 (Kubistin et al., 2010). Lelieveld et al. (2008) proposed that the missing OH in the model for GABRIEL may result from the neglect of potential OH producing channels in HO_2+RO_2 reactions. Production of OH in certain HO_2+RO_2 reactions has been observed directly by Dillon and Crowley (2008), and has been inferred by product studies (Hasson et al., 2004; Le Crane et al., 2006; Jenkin et al., 2007, 2008, 2010). Inclusion of OH production in reactions of HO_2 with peroxy radicals derived from isoprene ($ISOPO_2$) in the MECCA box model provided a marked improvement in model success for OH and HO_2 (Lelieveld et al., 2008; Kubistin et al., 2010). However, high branching ratios for OH producing channels (200 to 400 %) were required in the model, and generation of OH in reactions of HO_2 with RO_2 radicals has thus far only been observed for RO_2 radicals containing acyl, α-carbonyl, α-hydroxy or α-alkoxy functionalities (Hasson et al., 2004; Le Crane et al., 2006; Jenkin et al., 2007, 2008, 2010; Dillon and Crowley, 2008). The observed branching ratio for OH production from RO_2 radicals structurally similar to $ISOPO_2$ has been given an upper limit of 6 % (Dillon and Crowley, 2008). Thus this mechanism appears chemically unlikely.

Measurements of OH made during the Program of Regional Integrated Experiments on Air Quality over the Pearl River Delta of China (PRIDE-PDR) campaign in July 2006 were again found to be higher than those predicted by a box model by a factor of 3 to 5 at low NO concentrations (<1 ppb), although modelled HO_2 concentrations were in good agreement with observations (Hofzumahaus et al., 2009). Additional OH production in the model from HO_2+RO_2 reactions was insufficient to explain the model discrepancy for the PRIDE-PDR campaign, but an unidentified missing species in the model (X), which converts RO_2 to HO_2 and HO_2 to OH, could explain both the mean diurnal cycles of OH and HO_2 (Hofzumahaus et al., 2009). The nature of this missing compound remains unknown.

In our previous study as part of the African Monsoon Multidisciplinary Analysis (AMMA) campaign (Commane et al., 2010; Stone et al., 2010) we also found that modelled HO_2 concentrations were consistent with observed HO_2 even in high isoprene airmasses over the rainforest but were unable to investigate our understanding of OH concentrations owing to instrumental issues.

In conjunction with the aircraft HO_x measurements reported in this work for the Oxidant and Particle Photochemical Processes (OP3) campaign in Borneo in 2008, Whalley et al. (2011) and Edwards et al. (2011) made ground based measurements of OH, HO_2 and OH reactivity in the Sabah region of the Borneo rainforest. Analysis of these ground based measurements also indicates missing OH sources in this region (Pugh et al., 2010; Whalley et al., 2011; Edwards et al., 2011), and model calculations using a version of the Dynamically Simple Model of Atmospheric Chemical Complexity (DSMACC) described in this work also indicate missing OH sinks (Whalley et al., 2011; Edwards et al., 2011). While the missing OH source in the morning could potentially be explained if there were a buildup of HONO during the night, with subsequent photolysis during the morning (Whalley et al., 2011), the missing OH source in the afternoon appears to be related to isoprene (Pugh et al., 2011; Whalley et al., 2011; Edwards et al., 2011), and is consistent with results from the GABRIEL project (Kubistin et al., 2010; Lelieveld et al., 2008; Martinez et al., 2010). The combination of OH concentration and reactivity measurements by Whalley et al. (2011) and Edwards et al. (2011), however, enable greater constraint on the model, and indicate that the magnitude of the OH source required by previous studies (Butler et al., 2008; Hofzumahaus et al., 2009; Kubistin et al., 2010; Lelieveld et al., 2008) may be even bigger than previously thought owing to an underestimation of the OH sinks.

From these studies, there is, therefore, a growing body of evidence from field measurements of OH and HO_2 suggesting failures in our understanding of HO_x chemistry in environments characterised by a combination of low NO_x concentrations and high emissions of biogenic VOCs (Carslaw et al., 2001; Tan et al., 2001; Thornton et al., 2002; Ren et al., 2008; Butler et al., 2008; Kubistin et al., 2008; Lelieveld et al., 2008; Martinez et al., 2010; Hofzumahaus et al., 2009; Pugh et al., 2010; Whalley et al., 2011). In addition to these field studies there have been a number of recent experimental and theoretical studies indicating that the OH-initiated oxidation of isoprene under low NO_x conditions is poorly characterised and misrepresented (Peeters et al., 2009; Paulot et al., 2009; da Silva et al., 2010).

Chamber studies by Paulot et al. (2009) have shown that the reaction of OH with isoprene-hydroxy-hydroperoxides (ISOPOOH), produced in the reaction of isoprene derived peroxy radicals ($ISOPO_2$) with HO_2, can lead to the

formation of epoxide species with regeneration of OH under low NO_x conditions. Structurally similar epoxides were shown to lead to secondary aerosol formation, which may sequester gas phase carbon from the atmosphere and result in reduced OH loss in models due to a reduction in importance of reactions of OH with isoprene oxidation products (Paulot et al., 2009).

Modelling of HO_x measurements made in a Ponderosa pine plantation in Sierra Nevada in 2007 (Wolfe et al., 2011) during the Biosphere Effects on Aerosols and Photochemistry Experiment (BEARPEX) incorporated the isoprene epoxide scheme (Paulot et al., 2009) in the one-dimensional Chemistry of Atmosphere-Forest Exchange (CAFE) model. However, additional OH sources during hot periods when temperatures and VOC concentrations were high were still required, with a return of OH from peroxy-peroxy reactions being the chosen mechanism, similar to the work of Lelieveld et al. (2008) and Kubistin et al. (2010).

Theoretical investigation of the OH-initiated oxidation of isoprene by Peeters et al. (2009) suggest that there is a rapid equilibrium between initial radical products of the OH + isoprene reaction and their corresponding peroxy radicals produced on reaction with molecular oxygen, resulting in the greatest reaction flux through the fastest product forming pathway. Peeters et al. (2009) propose that the fastest pathways occur through unimolecular 1,6-H-shifts in two of the peroxy radicals, producing HO_2 and unsaturated hydroperoxy-aldehydes (HPALDs). The HPALD products are thought to photolyse rapidly during the day to produce OH, thereby increasing the expected yield of both OH and HO_2. Subsequent chemistry of the organic fragments of HPALD photolysis, resulting in rapid formation of photo-labile peroxy-acid-aldehydes (PACALDs), is also expected to further increase the OH and HO_2 yields (Peeters et al., 2009; Peeters and Muller, 2010; Nguyen et al., 2010). More minor reaction pathways of the initial isoprene peroxy radicals are also proposed to contribute to OH production, and similar mechanisms are suggested in the oxidation of methyl vinyl ketone (MVK) and methacrolein (MACR) (Peeters et al., 2009).

Unimolecular H-shifts in peroxy radicals derived from isoprene have also been proposed to result in formation of OH, HCHO and either MVK or MACR (depending on the peroxy radical isomer) on the basis of Density Functional Theory (DFT) calculations (da Silva et al., 2010). This mechanism therefore predicts OH formation without production of HO_2, but is expected to be relatively slow compared to the bimolecular reactions of the peroxy radicals with HO_2, and so may not represent a significant OH source in tropical forest environments (da Silva et al., 2010). Unimolecular decomposition processes producing OH have also recently been proposed to occur in the oxidation of glyoxal (da Silva, 2010a, 2011) and carboxylic acids (da Silva, 2010b).

A global modelling study by Stavrakou et al. (2010) using the IMAGESv2 global chemistry transport model has shown that the Peeters mechanism is able to reproduce average boundary layer concentrations of OH and HO_2 observed during GABRIEL and INTEX-A aircraft campaigns to within 30 %. Implementation of the Peeters mechanism in this model increased the modelled OH concentrations by a factor of up to 4 over densely vegetated areas, and increased the HO_2 concentrations by a factor between 2.5 and 3 (Stavrakou et al., 2010). The epoxide scheme (Paulot et al., 2009), however, gave increases in OH concentration by a factor of only 0.25 in the same model framework (Stavrakou et al., 2010) and could not replicate the observations.

This recent literature thus provides four main suggestions to explain the model underestimate of OH concentration:

1. $RO_2 + HO_2 \rightarrow OH$ (Hasson et al., 2004; Le Crane et al., 2006; Jenkin et al., 2007, 2008, 2010; Dillon and Crowley, 2008; Lelieveld et al., 2008; Kubistin et al., 2010)

2. $HO_2 + X \rightarrow OH$ (Hofzumahaus et al., 2009)

3. $ISOPOOH + OH \rightarrow IEPOX + OH$ (Paulot et al., 2009)

4. $ISOPO_2 \rightarrow HPALD + HO_2$; $HPALD + h\nu \rightarrow OH$ (Peeters et al., 2009; Peeters and Muller, 2010; Nguyen et al., 2010)

Archibald et al. (2010, 2011) investigated several of these using a box model based on the MCM and the global chemistry-transport models STOCHEM (Archibald et al., 2010) and UKCA (Archibald et al., 2011). These studies concentrated on the impact on OH concentrations, and the consequences for modelling past, present and future atmospheres, but suggest that the mechanisms implemented in the model would not be able to reconcile the models with laboratory and field data.

In this paper we investigate these mechanisms, using observations of OH, HO_2 and other observations made during the Oxidant and Particle Photochemical Processes (OP3) field campaign in Borneo in 2008. In Sect. 2 we outline the OP3 campaign and specifically describe the OH and HO_2 instrumentation. In Sect. 3 we describe the modeling framework. In Sect. 4 we describe the OH and HO_2 observations and in Sect. 5 we test a variety of mechanisms for isoprene oxidation. Finally in Sect. 6 we draw conclusions.

2 Oxidant and Particle Photochemical Processes campaign

The Oxidant and Particle Photochemical Processes (OP3) campaign took place in 2008, using a combination of ground and aircraft measurements during the campaign (Hewitt et al., 2009). Ground based measurements were made in two intensive periods in April–May and June–July at the Bukit Atur Global Atmospheric Watch station (5.0° N, 117.8° E) in Danum Valley in the Sabah region of the Borneo rainforest. Aircraft measurements were made onboard the UK FAAM
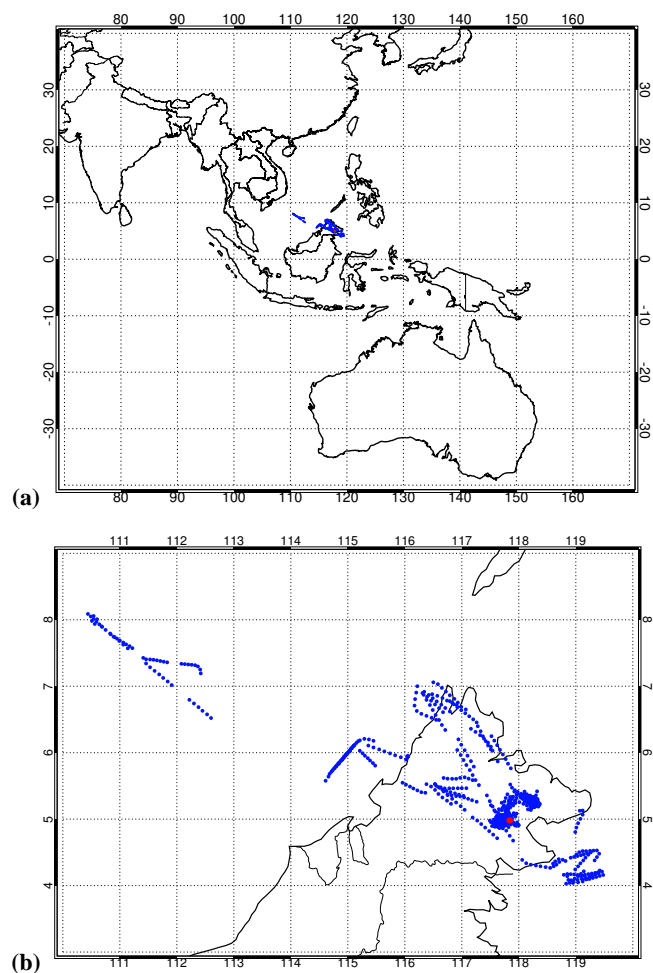
Fig. 1. Locations of the BAe146 aircraft during the OP3 campaign when OH or HO$_2$ data are available, showing **(a)** the wider geographical area and **(b)** a close up of the region of interest. The red point indicates the site of the ground based measurements in the rainforest during OP3.

BAe146 research aircraft, based at Kota Kinabalu International Airport during the campaign, from the 9 July to the 22 July 2008 to coincide with the ground based measurements.

Figure 1 shows the locations of the OH and HO$_2$ measurements made onboard the BAe146 during the campaign. Ten flights were made over Northern Borneo during OP3, with coverage of rainforest, oil palm and coastal sites. In general the observations showed high isoprene concentrations over the rainforest and oil palm plantations, with virtually no isoprene over the oceans (Hewitt et al., 2010; Jones et al., 2011). We focus here on the measurement and modelling of OH and HO$_2$ onboard the BAe146 during OP3, and provide a description of the Leeds AirFAGE instrument (Sect. 2.1). Details of supporting measurements (Sect. 2.2) used in this work are described in detail elsewhere (see Hewitt et al., 2009), and only brief descriptions are given here.

2.1 Detection of OH and HO$_2$

Measurements of OH and HO$_2$ were made using on-resonance pulsed Laser Induced Fluorescence (LIF) by the Fluorescence Assay by Gas Expansion (FAGE) technique (Hard et al., 1984; Heard and Pilling, 2003). The University of Leeds Aircraft FAGE instrument has been described in detail elsewhere (Commane et al., 2010), and only a brief description is given here.

Ambient air from the aircraft exterior is drawn into a fluorescence cell maintained at pressures ranging from 2.5 Torr at sea level to 1.5 Torr at 9 km. The fluorescence cell has two excitation axes, with excess NO added at the second excitation axis to titrate HO$_2$ to OH, enabling simultaneous detection of OH and HO$_2$. Laser light at $\lambda \sim 308$ nm, generated by a solid state Nd:YAG pumped Ti:Sapphire laser system (Bloss et al., 2003), is passed to the two excitation axes of the fluorescence cell, and to a reference cell, by fibre optic cables, and collimated and baffled before entering the cell. The beams exit the excitation regions of the cell through a baffled arm and are directed to a calibrated UV photodiode to provide a measurement of laser power.

Channel photomultiplier tubes (PMTs), situated perpendicular to both the air flow and excitation light axes and coupled to gated photon counters, detect interference filtered UV fluorescence from excited OH in both excitation regions, with the gated photon counters enabling separate measurements of fluorescence signal and scattered solar light. In order to prevent saturation of the PMTs resulting from detection of scattered laser light, PMT detection is also temporally gated, using a fast photodiode coupled to an oscilloscope to monitor the onset of the ~ 308 nm pulse from the Ti:Sapphire laser. During the African Monsoon Multidisciplinary Analysis (AMMA) campaign, the PMTs were gated with a constant time period between triggering of the Ti:Sapphire laser by the Nd:YAG laser and detection by the PMT (Commane et al., 2010). However, it has been shown that the time taken for the Ti:Sapphire to generate the 308 nm laser pulse after triggering can change significantly with fluctuations in temperature, with important consequences for instrument sensitivity (Commane et al., 2010; Whalley et al., 2010). Automatically monitoring the onset of the ~ 308 nm pulse enables fluorescence detection to be initiated by delivery of the laser pulse to the excitation cell, and not the time at which 308 nm generation is instigated by the Nd:YAG laser (Whalley et al., 2010). Introduction of this system for OP3 enabled any drift in the timing between the Nd:YAG and Ti:Sapphire lasers to be accounted for explicitly, and significantly reduced the effects of fluctuations in ~ 308 nm pulse generation times on instrument sensitivity.

A reference cell, in which OH radicals are produced by pyrolysis of water vapour in humidified cabin air passed over an electrically heated Ni:Chrome wire and receiving approximately 4 % of the total UV laser radiation, is used to determine the wavelength at which the OH fluorescence signal is
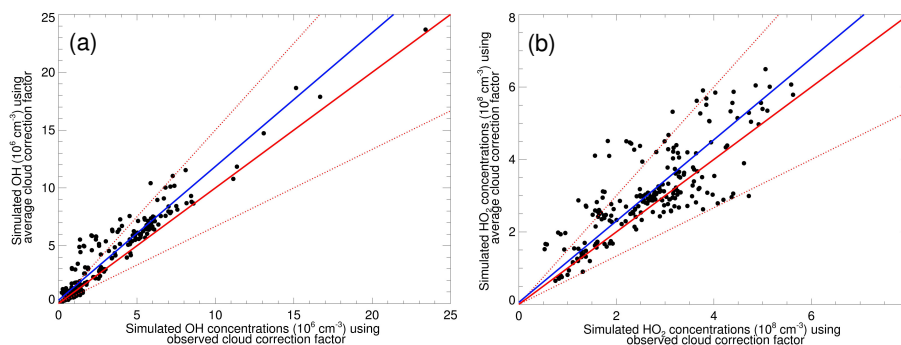
Fig. 2. Comparison of **(a)** OH and **(b)** HO$_2$ model concentrations between a model run using cloud correction factors determined for each data point from observations of j(NO$_2$) and a model run using a campaign average cloud correction factor (determined to be 0.74±0.24). The solid red lines represent the 1:1 line, with 50 % limits given by the broken red lines. The best fit lines are given in blue and are described by $y = (1.16\pm0.11)x + (0.29\pm0.48)$ for OH ($r^2 = 0.91$) and $y = (1.12\pm0.12)x + (0.06\pm0.34)$ for HO$_2$ ($r^2 = 0.64$).

at a maximum. Feedback to the stepper motor controlling the positioning of the diffraction grating within the Ti:Sapphire laser cavity and hence its wavelength enables optimisation of the signal intensity.

Calibration of the FAGE instrument is achieved by measurement of the signal from known concentrations of OH and HO$_2$ radicals, as described previously by Commane et al. (2010). Calibrations were performed over a range of conditions pertinent to the OP3 campaign. A value of 1.12×10^{-7} s^{-1} cm^3 mW^{-1} was determined for the instrument sensitivity to OH (C_{OH}), and 2.27×10^{-7} s^{-1} cm^3 mW^{-1} was determined for HO$_2$ (C_{HO_2}). No degradation of instrument sensitivity was observed between pre- and post-campaign calibrations. Average limits of detection for OH and HO$_2$ for 60 s sampling periods, calculated using the method described by Commane et al. (2010), were found to be 2.3×10^6 cm^{-3} and 2.0×10^6 cm^{-3}, respectively, with a 1σ calibration uncertainty of 28 % for OH and HO$_2$.

2.2 Supporting measurements

Details of supporting measurements onboard the BAe146 aircraft during OP3 are given in Hewitt et al. (2010). A brief description of measurements used to constrain the model is given below.

Ozone was measured using a TECO 49C UV absorption detector. Carbon monoxide measurements were made using an AeroLaser AL5002 Fast Carbon Monoxide Monitor (Gerbig et al., 1999). NO$_x$ measurements were made by a NO$_{xy}$ instrument (Brough et al., 2003; Stewart et al., 2008) measuring the chemiluminescence from the reaction between NO and O$_3$. NO$_2$ is converted to NO by photolysis to enable measurement of NO$_2$. Detection limits for the NO$_{xy}$ instrument are 3 ppt for NO and 15 ppt for NO$_2$ at an averaging time of 10 s.

Volatile organic compounds (VOCs) and oxygenated volatile organic compounds (oVOCs) were measured by both

Proton TRansfer Mass Spectrometry (PTRMS) (Capes et al., 2009; Murphy et al., 2010) and Gas Chromatography (GC) with a flame ionisation detector (Hopkins et al., 2006, 2009; Jones et al., 2011). Measurements by PTRMS were made approximately every 15 s, while those by GC were made approximately every 15 min throughout the flight via grab samples and subsequent off-line analysis. Isoprene and MVK and MACR measurements are available from both PTRMS and GC instruments, and model input uses the PTRMS measurement where available due to the higher time resolution.

Photolysis rates of NO$_2$ (j(NO$_2$)) and O$_3$ (j(O^{1}D)) were measured by fixed bandwidth radiometry, each with $2\times2\pi$-sr filter radiometers (Edwards and Monks, 2003). However, owing to instrumental problems during the campaign there are little data available for j(O^{1}D), and the overlap between measurements of HO$_x$ and j(NO$_2$) is limited. This offers a significant limitation in the number of points we can model. We have therefore used an average cloud correction factor for the campaign to maximise the number of data points available to model. The average cloud correction factor, determined as the average ratio of all the j(NO$_2$) observations to the clear skies j(NO$_2$) calculated by TUV, was found to be 0.74±0.24. Figure 2 shows the comparison between model simulations for OH and HO$_2$ using standard MCM v3.1 chemistry for a model run using cloud correction factors determined from observed j(NO$_2$) and a model run using the campaign average cloud correction factor. Strong correlations exist between the model simulations for both OH ($r = 0.91$) and HO$_2$ ($r = 0.64$). There is a slight overestimation of both species using the campaign average cloud correction factor ($\sim$12–15 %), but the extent of the overestimation is small compared to uncertainties in HO$_x$ observations ($\sim$28 % at the 1σ level) and other uncertainties in the model. In order to maximize the available data points we have run the model with the campaign average cloud correction factor.

3 Model approach

We have used the Dynamically Simple Model of Atmospheric Chemical Complexity (DSMACC) (Emmerson and Evans, 2009; Stone et al., 2010) for this study. DSMACC is a flexible zero-dimensional box model using the Kinetic Pre-Processor (KPP) (Sandu et al., 2006). The calculations described here use an observationally constrained version, which has been described previously in detail (Stone et al., 2010) and follows the approach of Jaegle et al. (2000) and Olson et al. (2004, 2006). The objective is to use the chemical scheme in the model to calculate an expected concentration of OH or HO_2 for each observation using the supporting measurements made onboard the aircraft. The base model uses a chemistry scheme described by the Master Chemical Mechanism version 3.1 (MCM v3.1) (Jenkin et al., 2003; Saunders et al., 2003) which contains near explicit degradation schemes for 135 volatile organic compounds in the troposphere, resulting in over 5600 species and 13 500 reactions and representing a detailed and comprehensive chemistry scheme for modelling tropospheric composition. Novel degradation mechanisms can be incorporated easily in DSMACC, enabling facile investigation of recently proposed changes to chemical schemes currently adopted for tropospheric modelling. Simulations reported here use degradation chemistry for methane, ethane, propane, *i*-butane, *n*-butane, ethene, propene, acetylene, acetaldehyde, methanol, acetone and isoprene. For all species, a removal reaction was also included which could be considered as a continuous deposition process (such as dry deposition or a continuous wet deposition), at a 1st order rate equivalent to a 24 h lifetime. Model sensitivity to this parameter is discussed in Stone et al. (2010) and is not found to be significant.

All aircraft measurements are merged onto a 60 s timebase for expediency. To be modelled, time points needed to have observations of OH or HO_2 together with the physical state (latitude, longitude, pressure, temperature and water vapour concentration) and observations of CO, O_3 and NO. Concentrations of CH_4 and H_2 were kept constant at values of 1770 ppb (GLOBALVIEW-CH4, 2009; ftp://ftp.cmdl.noaa.gov/ccg/ch4/) and 550 ppb (Ehhalt and Roher, 2009; Novelli et al., 1999) respectively. Where ethane, propane, *i*-butane, *n*-butane, ethene, propene, acetylene, methanol, acetone, isoprene, methyl vinyl ketone (MVK) and methacrolein (MACR) were available they were also included.

In order to maximise the number of points in the model, any data where measurements of VOCs were not available we used parameterised concentrations of alkanes (ethane, propane, *i*-butane, *n*-butane), alkenes (ethene and propene) and alkynes (acetylene) as a linear function of the CO concentration, as described in our previous work (Stone et al., 2010). Table 1 shows the fitting parameters used in this procedure. A summary of inputs to the model is given in Table 2.

For each observed time point, those species which have been observed are set to the observed value and kept con-

Table 1. Parameters used to fit hydrocarbon data as a function of the CO concentration. Hydrocarbon concentrations were used in ppt, while CO concentrations were in ppb. RMS refers to the root mean square difference between the observed and calculated values.

Hydrocarbon/ppt	Linear regression	r^2	RMS/ppt
Ethane	$(6.61 \times [CO]/ppb) - 54.17$	0.217	4.92
Propane	$(2.76 \times [CO]/ppb) - 73.39$	0.144	11.74
iso-butane	$(0.52 \times [CO]/ppb) - 17.09$	0.056	18.01
n-butane	$(1.12 \times [CO]/ppb) - 49.74$	0.133	16.63
Ethene	$(4.30 \times [CO]/ppb) - 130.98$	0.162	10.35
Propene	$(1.00 \times [CO]/ppb) - 40.24$	0.264	15.12
Acetylene	$(4.36 \times [CO]/ppb) - 115.14$	0.372	9.06

Table 2. Summary of data inputs to the model. Chemical names are those used in the MCM.

Species	Mean	Median	Range
O_3/ppb	13.9 ± 3.2	13.7	7.0–24.0
CO/ppb	67.4 ± 10.1	64.8	43.7–105.7
H_2O/ppm	$18\,340 \pm 8982$	18 738	2212–30 773
NO/ppt	52.6 ± 109.0	30.3	0.02–1239.4
NO_2/ppt	146.0 ± 215.4	78.4	0–1908.5
$j(NO_2)/10^{-3}\,s^{-1}$	8.1 ± 1.7	8.2	2.7–10.5
C_2H_6/ppt	394.9 ± 68.4	377.9	236.5–644.8
C_3H_8/ppt	115.1 ± 30.3	107.6	42.2–218.6
iso-C_4H_{10}/ppt	17.6 ± 6.5	16.3	2.8–84.9
n-C_4H_{10}/ppt	25.75 ± 12.1	22.8	0–68.5
C_2H_4/ppt	162.0 ± 57.5	148.0	17.7–450.0
C_3H_6/ppt	26.4 ± 11.2	24.0	5.5–65.2
C_2H_2/ppt	181.2 ± 48.1	168.3	51.6–448.6
CH_3OH/ppt	480.1 ± 1200.1	0	0–7102.9
CH_3COCH_3/ppt	294.4 ± 668.5	0	0–5238.3
C_5H_8/ppt	783.8 ± 1575.1	36.3	0–13 249.0
MVK/ppt	420.2 ± 580.3	71.4	0–2567.6
MACR/ppt	64.5 ± 106.1	2.94	0–511.1

stant. Those species which have not been observed or parameterised as a function of CO are set initially to zero. Concentrations of NO_x are constrained using the method described previously by Stone et al. (2010). Over each 24 h period in the model the concentration of each individual NO_x species varies according to its photochemistry, but the total NO_x concentration is kept constant. At the end of each 24 h period the calculated concentration of NO is compared to its measured concentration and the concentration of all NO_x species is fractionally increased or decreased so that the measured and modelled concentrations of NO match. The model is integrated forwards in time with diurnally varying photolysis rates until a diurnal steady state is reached, typically requiring between 5 and 10 days.
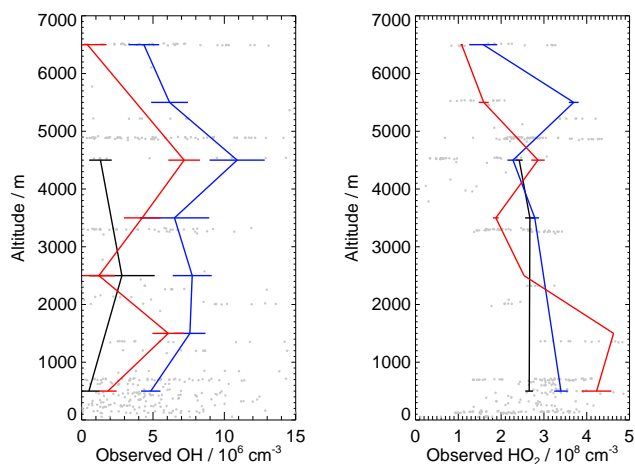
Fig. 3. Observed concentrations of **(a)** OH and **(b)** HO$_2$ during the OP3 aircraft campaign as a function of altitude (grey points) averaged over 1 min. Mean concentrations and the standard error in 1000 m altitude bins are shown for observations from (local time) 07:30 to 10:30 h (black), 10:30 to 13:30 h (blue) and 13:30 to 16:30 h (red).

4 Observations of OH and HO$_2$

OH and HO$_2$ were measured on six flights throughout the campaign over rainforest, oil palm plantation and coastal and ocean regions, providing approximately 35 h of data (Hewitt et al., 2010). Owing to the model requirements for supporting data (e.g. O$_3$, CO, NO) we simulate 600 of the 763 HO$_x$ data points available on a 1 min timescale. Since not all available HO$_x$ data are used in the model a brief overview is given here to highlight the entire dataset. The locations of these observations are shown in Fig. 1.

The variation of OH and HO$_2$ with altitude is shown in Fig. 3. Concentrations of OH and HO$_2$ were generally above the 1σ 60 s limit of detection throughout the campaign (2.3×10^6 cm^{-3} for OH and 2.0×10^6 cm^{-3} for HO$_2$), although those for OH were nearer to the detection limit than for HO$_2$. Concentrations of OH were found to be highly variable with altitude, reflecting both instrumental noise and the complexity of the processes responsible for determining atmospheric OH concentrations. Concentrations of HO$_2$ tend to decrease with increasing altitude, with similar results obtained in previous aircraft campaigns (Mao et al., 2009; Ren et al., 2008; Martinez et al., 2010).

Figure 3 shows the altitude dependence of OH and HO$_2$ at different times of day. Mean OH concentrations were higher around noontime than in the morning or afternoon at all altitudes. Mean HO$_2$ concentrations were highest around noontime in the boundary layer, but the mean noontime HO$_2$ concentrations at higher altitudes were lower than those observed during the afternoon. Mean concentrations between 1100 and 1300 during OP3 in the boundary layer

(z<2000 m) were found to be (5.28±6.02)×10^6 cm^{-3} for OH and (3.54±0.84)×10^8 cm^{-3} for HO$_2$.

In Sect. 5 we investigate the ability of the DSMACC box model to simulate the observations of OH and HO$_2$ made during OP3 as a test of our understanding of isoprene photochemistry in low NO$_x$ regions. A significant advantage of aircraft data over ground-based data for these purposes is the dynamic range of physical and chemical conditions covered by the aircraft, providing a much wider range of conditions over which we can test our understanding.

5 Model results

The ability of the model to successfully simulate OH and HO$_2$ is linked to the quality (noise, bias etc.) of model input parameters and the quality of the OH and HO$_2$ observations themselves. If the objective of this paper were an overall assessment of our understanding of the OH concentration the noise and bias of the input parameters and HO$_x$ observations would be important. However, the specific focus of this study is the investigation of the ability of the model to simulate isoprene photochemistry. Thus, "success" with the model in this case would be a model performance for HO$_x$ which is independent of the isoprene concentration regardless of the noise or bias associated with the observations.

Our primary tool for this assessment is the ratio between the observed and modelled OH or HO$_2$ concentration. Unless otherwise stated the statistics are applied to the log$_{10}$ of this ratio and then converted back by raising the appropriate result of the statistic to the power of 10. This provides significant advantages over using the ratio alone. For example, for three model points which have observed to modelled ratios of 0.1, 1 and 10 the mean of these values is 3.7. However, this fails to reflect that the model performance is equally "bad" at a ratio of 0.1 as it is at 10. Performing the statistics on the log of these values $10^{[(\log_{10}(0.1)+\log_{10}(1)+\log_{10}(10)]/3}$ gives a value of 1 which better reflects the model performance, which in this example is noisy but not biased. We define three primary metrics for our model simulations and report their values in Table 3.

1. The mean observed to modelled average ratios ($10^{\text{mean}(\log_{10}(\text{ratio}))}$) for OH and HO$_2$ for observational points with isoprene greater than 15 ppt and for points with isoprene concentrations less than 15 ppt. We choose the value of 15 ppt to represent the point at which isoprene has a significant impact on the photochemistry. At a concentration of 15 ppt, isoprene represents 10 % of the rate of loss of OH compared to the rate of loss of OH to CO at the median observed CO concentration (65 ppb). These average ratios are shown in Table 3. Variations around the mean are described as ($10^{\text{mean}(\log_{10}(\text{ratio}))\ \pm\ \text{standard deviation}(\log_{10}(\text{ratio}))}$).
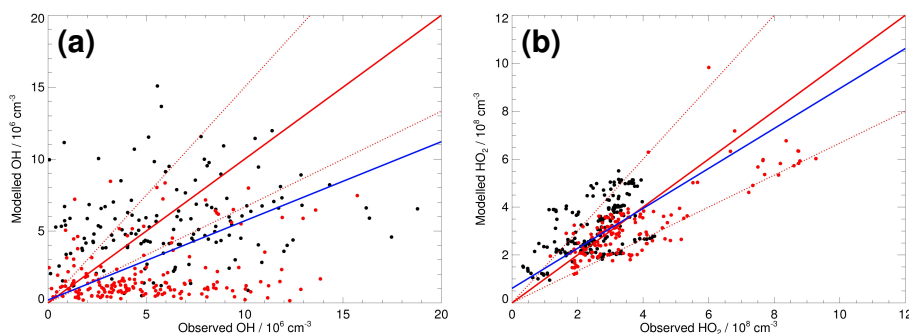
Fig. 4. Comparison between modelled and observed concentrations of **(a)** OH and **(b)** HO_2 for the base MCM model run. Observations shown are 60 s averages. Points in red are those with isoprene concentrations greater than 15 ppt, while those in black have isoprene concentrations less than 15 ppt. The solid red lines represent the 1:1 line, with 50 % limits given by the broken red lines. The best fit lines are given in blue and are described by $[OH]_{mod} = (0.55\pm0.09)[OH]_{obs} + ((0.20\pm0.59)\times10^6)$ with $r^2 = 0.05$ and $[HO_2]_{mod} = (0.83\pm0.08)[HO_2]_{obs} + ((0.61\pm0.25)\times10^8)$ with $r^2 = 0.45$.

Table 3. Mean observed to modelled ratios of OH and HO_2 at isoprene concentrations above and below 15 ppt for each mechanism. Errors shown are the standard deviations in the mean. P_D refers to the probability result of the Kolmorogov-Smirnov test and refers to the probability that the distribution functions of the ratios for data points with isoprene above and below 15 ppt are statistically identical. P_H refers to the probability result of the Kruskal-Wallis test and indicates the probability that the ratios for data points with isoprene concentrations above 15 ppt are independent of the isoprene concentration. Probability values less than 0.001 are listed as zero. MCM v3.2 was launched during the preparation of this manuscript and results are included in the table. MCM results referred to in the text refer to those using MCM v3.1.

Mechanism	Mean $[OH]_{obs/mod}$, $C_5H_8 < 15$ ppt	Mean $[OH]_{obs/mod}$, $C_5H_8 > 15$ ppt	P_D	P_H	Mean $[HO_2]_{obs/mod}$, $C_5H_8 < 15$ ppt	Mean $[HO_2]_{obs/mod}$, $C_5H_8 > 15$ ppt	P_D	P_H
MCM v3.1	$1.62^{+1.27}_{-1.24}$	$5.32^{+3.68}_{-4.43}$	0	0	$0.86^{+0.32}_{-0.31}$	$1.18^{+0.30}_{-0.30}$	0	0.921
MCM v3.2	$1.62^{+1.27}_{-1.24}$	$4.51^{+3.08}_{-3.75}$	0	0	$0.83^{+0.31}_{-0.31}$	$1.05^{+0.27}_{-0.27}$	0	0.889
$C_5H_8 + OH$ $\rightarrow 3$ OH	$1.62^{+1.27}_{-1.24}$	$1.62^{+1.25}_{-1.25}$	0.867	0.054	$0.86^{+0.32}_{-0.31}$	$0.67^{+0.30}_{-0.26}$	0	0
$HO_2 + ISOPO_2$ $\rightarrow 3$ OH	$1.62^{+1.27}_{-1.24}$	$1.62^{+1.11}_{-1.21}$	0.913	0.149	$0.86^{+0.32}_{-0.31}$	$0.70^{+0.21}_{-0.21}$	0	0
$HO_2 + RO_2$ $\rightarrow 0.5$ OH	$1.42^{+1.14}_{-1.07}$	$4.13^{+2.87}_{-3.39}$	0	0	$0.81^{+0.30}_{-0.30}$	$1.05^{+0.27}_{-0.27}$	0	0
$RO_2 + X \rightarrow HO_2$ $HO_2 + X \rightarrow OH$	$1.62^{+1.27}_{-1.24}$	$1.68^{+0.38}_{-1.49}$	0	0.001	$0.86^{+0.32}_{-0.31}$	$0.89^{+0.40}_{-0.40}$	0.002	0
Epoxide	$1.62^{+1.27}_{-1.24}$	$4.27^{+2.90}_{-3.52}$	0	0	$0.86^{+0.32}_{-0.31}$	$0.96^{+0.24}_{-0.24}$	0	0.633
da Silva	$1.62^{+1.27}_{-1.24}$	$5.19^{+3.61}_{-4.31}$	0	0	$0.86^{+0.32}_{-0.31}$	$1.17^{+0.30}_{-0.30}$	0	0.943
Peeters	$1.62^{+1.27}_{-1.24}$	$1.50^{+1.12}_{-1.14}$	0.820	0.014	$0.86^{+0.32}_{-0.31}$	$0.46^{+0.18}_{-0.19}$	0	0

2. Although the average observed to modelled ratio provides useful information, it fails to represent all of the information available regarding model success or failure. To describe more of this information the probability distribution functions (PDFs) of the logarithm of the observed to modelled ratio are calculated again for both OH and HO_2, separating those points with isoprene concentrations less than 15 ppt from those points with isoprene concentrations greater than 15 ppt (see Fig. 5). A "successful" model would show no significant differ-

ence between the distributions with low and high isoprene concentrations. The goodness of fit between the two PDFs is defined using a Kolmogorov-Smirnov test (Kolmogorov, 1933; Smirnov 1948; Stephens, 1974) and the values are shown in Table 3.

3. We take this analysis further in a third metric. A "success" for the model should also be independent of the isoprene concentration. Thus a successful model with respect to isoprene should lead to the same average observed to modelled OH and HO_2 ratios at all isoprene
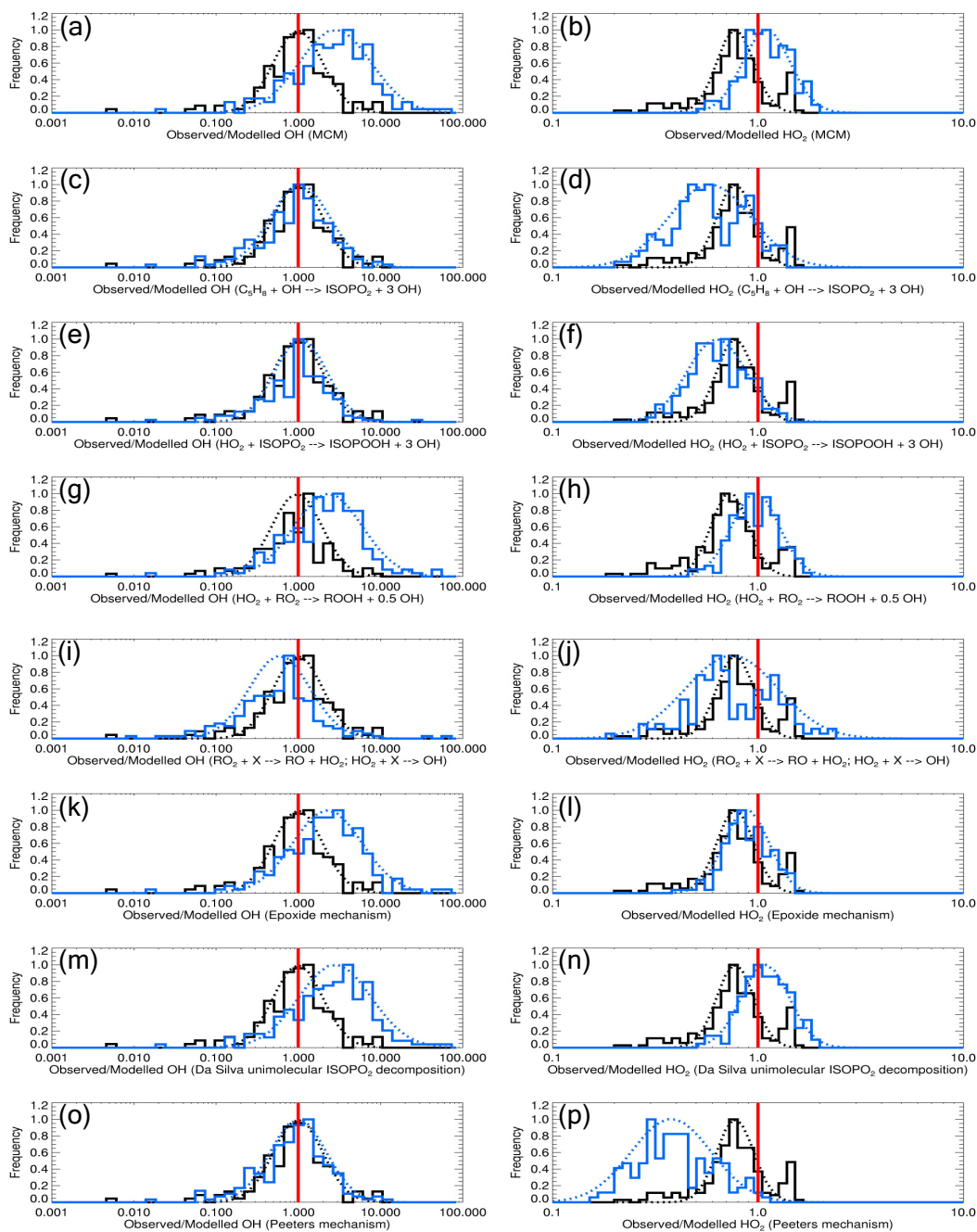
Fig. 5. Probability distribution functions for observed to modelled ratios of OH (left hand side) and HO$_2$ (right hand side) for each mechanism implemented in the model. Broken lines show a Gaussian fit to the probability density functions, with data points with isoprene below 15 ppt shown in black and those with isoprene above 15 ppt shown in blue. The red line indicates an observed to modelled ratio of 1. Plot **(a)** is for OH using the base MCM; **(b)** HO$_2$ using the base MCM; **(c)** OH using the simple recycling scheme OH + C$_5$H$_8$ → ISOPO$_2$ + 3 OH; **(d)** HO$_2$ using OH + C$_5$H$_8$ → ISOPO$_2$ + 3 OH; **(e)** OH using HO$_2$ + ISOPO$_2$ → ISOPOOH + 3 OH; **(f)** HO$_2$ using HO$_2$ + ISOPO$_2$ → ISOPOOH + 3 OH; **(g)** OH using HO$_2$ + RO$_2$ → ROOH + 0.5 OH; **(h)** HO$_2$ using HO$_2$ + RO$_2$ → ISOPOOH + 0.5 OH; **(i)** OH invoking the missing species X to convert RO$_2$ to HO$_2$ and HO$_2$ to OH; **(j)** HO$_2$ invoking the missing species X to convert RO$_2$ to HO$_2$ and HO$_2$ to OH; **(k)** OH using the epoxide mechanism (Paulot et al., 2009); **(l)** HO$_2$ using the epoxide mechanism (Paulot et al., 2009); **(m)** OH using unimolecular decomposition of β-ISOPO$_2$ (da Silva et al., 2010); **(n)** HO$_2$ using unimolecular decomposition of β-ISOPO$_2$ (da Silva et al., 2010); **(o)** OH using the Peeters mechanism (Peeters et al., 2009; Peeters and Muller, 2010); **(p)** HO$_2$ using the Peeters mechanism (Peeters et al., 2009; Peeters and Muller, 2010). See text for further details regarding each scheme.

concentrations. For those points with isoprene greater than 15 ppt we assess the differences in the average observed to modelled HO_x ratios for isoprene concentrations between 15 and 100 ppt, 100 to 1000 ppt and those above 1000 ppt. This is shown graphically in Fig. 6. A Kruskal-Wallis H-test (Kruskal and Wallis, 1952) is used to assess whether the average ratio in each of the isoprene bins is sampled from the same population, and thus the statistical differences between the average ratios for each of the isoprene bins. The values of this statistic are represented in Table 3.

5.1 Master chemical mechanism

Figure 4a shows the point by point DSMACC model performance for OH using standard MCM v3.1 chemistry. Points have been coloured to show those with isoprene concentrations above and below 15 ppt (red and black, respectively). There is significant underestimation of OH by the model for those points with isoprene above 15 ppt, consistent with model studies of previous field campaigns in similar high isoprene and low NO_x environments (Lelieveld et al., 2008; Hofzumahaus et al., 2009; Ren et al., 2008).

There is a clear separation of the maxima of the probability distribution functions of the observed to modelled ratios of OH for data points with observed isoprene concentrations above and below 15 ppt, with a mean observed to modelled OH ratio of $1.62^{+1.27}_{-1.24}$ for data points with isoprene less than 15 ppt and a mean ratio of $5.32^{+3.68}_{-4.43}$ for data points with isoprene concentrations greater than 15 ppt, as shown in Fig. 5a. Those points "without" isoprene show much better performance.

Figure 4b shows the model performance for HO_2 using MCM chemistry. We find that observations of HO_2 are generally lower than the model at low or zero isoprene concentrations, with a mean observed to modelled ratio of $0.86^{+0.32}_{-0.31}$, but higher than the model at higher isoprene concentrations, with a mean ratio of $1.18^{+0.30}_{-0.30}$.

Results of the Kolmogorov-Smirnov test, shown in Table 3, indicate a significant difference between the distribution functions for the OH ratios for points with isoprene above and below 15 ppt. Figure 6 shows the observed to modelled HO_x ratios as a function of the isoprene concentration, and the Kruskal-Wallis H-test (Fig. 6a and Table 3) shows that the model failure for OH is significantly worse for those points with high isoprene concentrations than for those with low isoprene.

The probability distribution functions for observed to modelled ratios of HO_2 are also shown in Fig. 5b. The Kolmogorov-Smirnov test (Table 3) shows that the differences between the distribution functions for HO_2 are significant, but the Kruskal-Wallis test (Fig. 6b, Table 3) demonstrates that there are no statistical differences between the observed to modelled ratios of HO_2 for points with isoprene concentrations above 15 ppt. This result indicates that al-

though there is a difference in the modelled HO_2 between those points with isoprene below 15 ppt and those with isoprene above 15 ppt, there is no systematic dependence of model success for HO_2 on the isoprene concentration, similar to our previous work during the African Monsoon Multidisciplinary Analyses (AMMA) campaign (Commane et al., 2010; Stone et al., 2010).

The model results for OH are consistent with those obtained for previous field campaigns (Lelieveld et al., 2008; Hofzumahaus et al., 2009; Ren et al., 2008), with a significant underestimate of OH and much better agreement for HO_2. The instantaneous OH budget for a single typical rainforest data point shown in Fig. 7a reveals that reaction with isoprene is the dominant sink for OH in the model. This reaction is responsible for 63.7 % of the total OH loss. Results for the GABRIEL campaign found OH + isoprene to be responsible for 62 % of the OH loss in the boundary layer over land in the afternoon (Kubistin et al., 2010). Figure 7a also shows that reactions of OH with oxidation products of isoprene, such as organic peroxides and HCHO, constitute significant loss processes for OH in the model. Figure 7b shows the HO_2 budget for the same point. This shows that loss of HO_2 is dominated by reactions of HO_2 with NO (45 %), $ISOPO_2$ (23 %) and HO_2 (21 %), while the sources of HO_2 are dominated by reactions of ISOPO with O_2 and photolysis of HCHO.

The existence of interference signals in FAGE measurements of OH and HO_2 were the subject of an extensive investigation by Ren et al. (2004), and could occur as a result of the fluorescence of a species with narrow absorption band lines in the same wavelength region as OH, or as a result of the production of OH by the excitation laser and its subsequent fluorescence. Both possibilities were investigated by Ren et al. (2004), and while the probability of such interference signals is deemed to be low, the potential for an interference signal from an unknown species cannot be entirely ruled out.

During the preparation of this manuscript, Fuchs et al. (2011) have shown the possibility of an interference in FAGE HO_2 measurements from alkene-derived RO_2 radicals. These species may react with the NO added to titrate HO_2 to OH during HO_2 FAGE measurements, resulting in the production of OH in the detection cell from radicals other than HO_2. Fuchs et al. (2011) show that interferences are possible from RO_2 radicals derived from a number of unsaturated hydrocarbons, including isoprene, and its oxidation products MVK and MACR. Any potential interference will be extremely dependent on the precise experimental configuration of the FAGE instrument in question, for example the residence time of sampled gas within the detection cell and relative positions of the NO injector and excitation laser beam. As shown in Fig. 6b and discussed above, there is no dependence of the observed to modelled ratio for HO_2 as a function of the observed isoprene concentration, with similar results observed in our previous work from the same aircraft
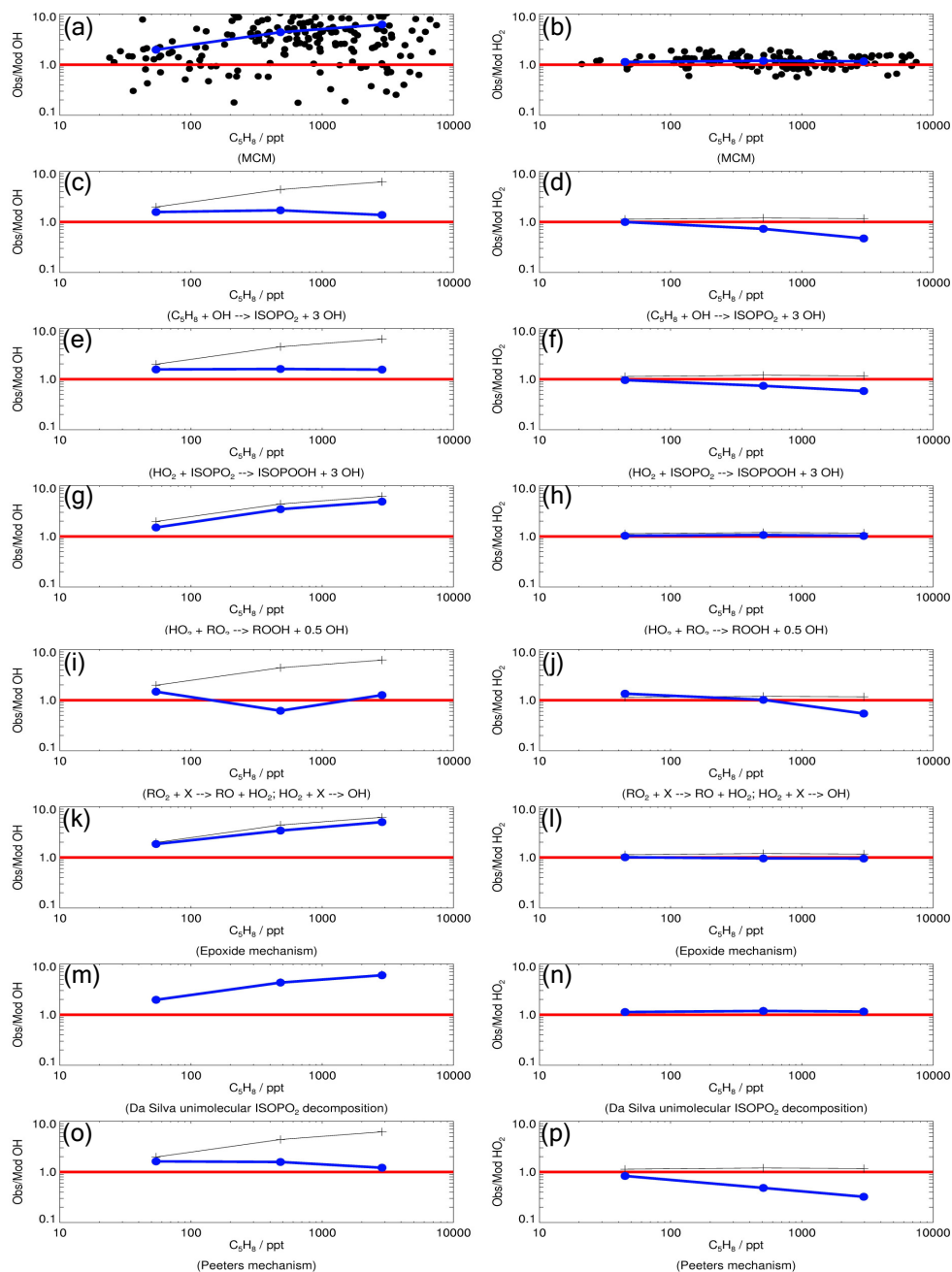
Fig. 6. Ratios of observed to modelled OH (left hand side) and HO_2 (right hand side) at isoprene concentrations 10 to 100 ppt, 100 to 1000 ppt and 1000 to 10 000 ppt for each mechanism implemented in the model (shown in blue). The thin black line shown on each plot represents the results for the base MCM run, with the red line indicating an observed to modelled ratio of 1. Raw data for the MCM base run (panels **a** and **b**) are shown, although it should be noted some data points have observed to modelled ratios for OH greater than 10 and are not shown for clarity. Plot **(a)** is for OH using the base MCM; **(b)** HO_2 using the base MCM; **(c)** OH using the simple recycling scheme $OH + C_5H_8 \rightarrow ISOPO_2 + 3OH$; **(d)** HO_2 using $OH + C_5H_8 \rightarrow ISOPO_2 + 3OH$; **(e)** OH using $HO_2 + ISOPO_2 \rightarrow ISOPOOH + 3OH$; **(f)** HO_2 using $HO_2 + ISOPO_2 \rightarrow ISOPOOH + 3OH$; **(g)** OH using $HO_2 + RO_2 \rightarrow ROOH + 0.5OH$; **(h)** HO_2 using $HO_2 + RO_2 \rightarrow ISOPOOH + 0.5OH$; **(i)** OH invoking the missing species X to convert RO_2 to HO_2 and HO_2 to OH; **(j)** HO_2 invoking the missing species X to convert RO_2 to HO_2 and HO_2 to OH; **(k)** OH using the epoxide mechanism (Paulot et al., 2009); **(l)** HO_2 using the epoxide mechanism (Paulot et al., 2009); **(m)** OH using unimolecular decomposition of β-$ISOPO_2$ (da Silva et al., 2010); (n) HO_2 using unimolecular decomposition of β-$ISOPO_2$ (da Silva et al., 2010); **(o)** OH using the Peeters mechanism (Peeters et al., 2009; Peeters and Muller, 2010); **(p)** HO_2 using the Peeters mechanism (Peeters et al., 2009; Peeters and Muller, 2010). See text for further details regarding each scheme.

Fig. 7. Processes controlling the instantaneous production (blue) and loss (red) rates for a typical data point over the rainforest for OH (left hand side) and HO_2 (right hand side). Plot **(a)** is for OH using the MCM; **(b)** HO_2 using the MCM; **(c)** OH using $HO_2 + ISOPO_2 \rightarrow ISOPOOH + 3\,OH$; **(d)** HO_2 using $HO_2 + ISOPO_2 \rightarrow ISOPOOH + 3\,OH$; **(e)** OH using the epoxide mechanism (Paulot et al., 2009); **(f)** HO_2 using the epoxide mechanism (Paulot et al., 2009); **(g)** OH using the Peeters mechanism (Peeters et al., 2009; Peeters and Muller, 2010); **(h)** HO_2 using the Peeters mechanism (Peeters et al., 2009; Peeters and Muller, 2010). The NO concentration for this data point was 42 ppt. Names are as used in the MCM or described in Tables 5 and 7.

over forested regions in West Africa (Commane et al., 2010; Stone et al., 2010). These results provide some support that any such interference for the Leeds AirFage instrument does not significantly alter the major findings of these studies.

In the introduction a number of different explanations for model discrepancies in regions with high biogenic emissions and low NO_x concentrations were given. We now implement these into our model and investigate the impact.

5.2 $C_5H_8 + OH \rightarrow ISOPO_2 + n\,OH$

A simple, but chemically unlikely, recycling scheme in which OH is produced directly by isoprene + OH (C_5H_8 + $OH \rightarrow ISOPO_2 + n\,OH$) was investigated to determine the extent of OH recycling required for the GABRIEL campaign (Kubistin et al., 2010). The best fit between the observation and the model required $n = 1.3$ (Kubistin et al., 2010).
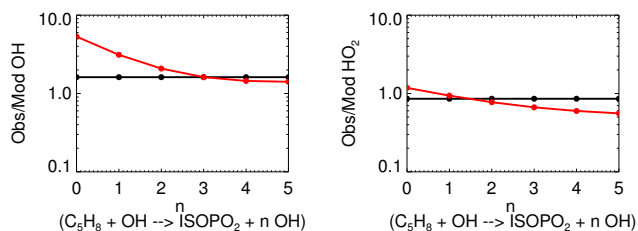
Fig. 8. Mean observed to modelled ratios of OH (left hand side) and HO_2 (right hand side) as a function of n, the extent of OH recycling in the simple scheme $OH + C_5H_8 \rightarrow ISOPO_2 + n$ OH. Points shown in black correspond to data points with isoprene below 15 ppt while those shown in red correspond to data points with isoprene above 15 ppt.

A series of model runs were conducted in which OH was directly regenerated in the reaction $C_5H_8 + OH \rightarrow ISOPO_2 + n$ OH, varying the yield of OH between 1 and 5 in integer steps. Figure 8 shows the mean observed to modelled ratios for OH and HO_2 as a function of n (the extent of OH recycling). We find that simulations for OP3 require production of approximately 3 OH for each OH radical lost in reaction with isoprene in order to optimise model success for OH, giving no significant differences in the $\log_{10}$ mean observed to modelled ratios for OH as a function of the isoprene concentration (Figs. 5c, 6c, Table 3).

Our optimal value of $n = 3$ is significantly higher than the values found in the GABRIEL study ($n = 1.3$, Kubistin et al., 2010).

However, we find that improvements in model success for OH using this method are gained at the expense of agreement for HO_2, with Fig. 6d showing that the ability to simulate HO_2 deteriorates with increasing isoprene concentration using this mechanism.

5.3 $HO_2 + RO_2 \rightarrow OH$

Production of OH in $HO_2 + RO_2$ reactions has been observed experimentally (Hasson et al., 2004; Le Crane et al., 2006; Jenkin et al., 2007, 2008, 2010; Dillon and Crowley, 2008), and production of between 2 and 4 OH radicals in $HO_2 + ISOPO_2$ reactions was used to rectify the model discrepancy found in the GABRIEL campaign (Lelieveld et al., 2008; Butler et al., 2008; Kubistin et al., 2010). Wolfe et al. (2011) also used this mechanism to rectify the model discrepancy for OH observed for the BEARPEX campaign using the CAFE model, invoking production of 2.6 OH from reactions of HO_2 with peroxy radicals derived from isoprene and 2-methyl-3-buten-2-ol.

We present results from a simulation incorporating production of 3 OH radicals from $HO_2 + ISOPO_2$ for all $ISOPO_2$ radicals in the MCM, in keeping with OH yields required to rectify the model discrepancies reported in previous studies (Lelieveld et al., 2008; Butler et al., 2008; Kubistin et al.,

2010; Wolfe et al., 2011). Figures 5e and 6e show the effects of this additional OH source in the model, revealing a significant improvement to the simulated OH. Table 3 shows the results of the statistical analyses for this model run. The Kolmogorov-Smirnov test on the mean observed to modelled OH ratios for points with isoprene above and below 15 ppt indicates that there is no statistical difference between the two regimes (Fig. 5e). Figure 6e and the Kruskal-Wallis test shows there is little dependence of OH model success on the observed isoprene concentration. Thus the problem with the modelled OH appears to be rectified by the inclusion of the reaction.

However, the modelled HO_2 concentrations are also increased as a result of this additional OH source, with an increase in the median modelled HO_2 concentration by a factor of 1.8 compared to the base MCM run. The probability distribution functions for HO_2 in Fig. 5f and observed to modelled ratios for HO_2 as a function of isoprene in Fig. 6f, and accompanying statistical tests in Table 3, show that a significant difference remains between the observed to modelled HO_2 ratio at isoprene concentrations below 15 ppt and that at isoprene concentrations above 15 ppt.

Figure 7d shows the HO_2 budget for the single point used in Fig. 7b. Comparison of the HO_2 budgets for the mechanism involving OH production from $HO_2 + ISOPO_2$ with the MCM run shows a much greater flux of HO_2 for the run including the additional OH production due to additional HO_2 production from intermediates formed by OH + VOC reactions.

While this mechanism may replicate the OH concentrations, a branching ratio for OH production of 300 % is far greater than experimental observations suggest, particularly for $ISOPO_2$ radicals, for which structural analogues suggest an upper limit to the branching ratio for OH production of only 6 % (Dillon and Crowley, 2008). OH production in $HO_2 + RO_2$ reactions has thus far only been observed for RO_2 radicals containing acyl, α-carbonyl, α-hydroxy or α-alkoxy functionalities (Hasson et al., 2004; Le Crane et al., 2006; Jenkin et al., 2007, 2008, 2010; Dillon and Crowley, 2008).

Figures 5g–h and 6g–h display the results from a simulation in which production of OH was included for all $HO_2 + RO_2$ reactions with a more realistic branching ratio of 50 %. Even without limiting OH production to RO_2 radicals containing acyl, α-carbonyl, α-hydroxy or α-alkoxy functionalities the lower branching ratio cannot replicate the OH observations made during OP3.

It therefore seems chemically unlikely that production of OH from $HO_2 + RO_2$ chemistry offers a mechanistic explanation for these results.

5.4 $RO_2 \rightarrow HO_2 \rightarrow OH$

Hofzumahaus et al. (2009) reconciled model discrepancies observed for OH during the PRIDE-PDR campaign by introduction of an unidentified missing species (X) in the model

which converts RO_2 to HO_2 and HO_2 to OH, similarly to the effects of NO but without production of ozone. We have investigated this possibility by inclusion of the reactions $HO_2 + X \rightarrow OH$ and $RO_2 + X \rightarrow RO + HO_2$, occurring with the rate coefficients k_{HO_2+X} and k_{RO_2+X}, respectively. Given the relationship between model failure and isoprene concentration, the concentration of X was set to be equal to that of isoprene. Optimisation of model success was achieved by variation of k_{HO_2+X} and k_{RO_2+X} to give statistically similar mean observed to modelled ratios of OH and HO_2 for data points with isoprene above and below 15 ppt.

Figures 5i–j and 6i–j show the results for the optimised model run. Although we are able to find agreement in the $\log_{10}$ mean observed to modelled ratios for OH and HO_2 (Fig. 5i–j), we are unable to find a result that gives statistically similar modelled to observed HO_x distribution functions in the Kolmogorov-Smirnov test (P_D in Table 3) or statistically similar observed to modelled HO_x ratios as a function of isoprene in the Kruskal-Wallis test (Fig. 6i–j and P_H in Table 3).

In order to achieve the statistically similar mean observed to modelled HO_x ratios we require values of $k_{HO_2+X}[X]$ = $(1.81\pm2.12)\,s^{-1}$ and $k_{RO_2+X}[X] = (0.04\pm0.05)\,s^{-1}$. For ground-based measurements made during OP3 within the rainforest in April 2008, 0.74 ppb of an NO equivalent (i.e. converting HO_2 to OH at an equivalent rate to that of NO) was required to replicate the average observed OH diurnal profile (Whalley et al., 2011). This gives an approximate value of $k_{HO_2+X}[X] = 0.16\,s^{-1}$. Although this value is lower than that required here, the observed isoprene concentration at the ground-based rainforest site was typically lower ($\sim$2 ppb maximum) than the mean observed isoprene concentration measured during the aircraft campaign (1–3 ppb over the rainforest and 5–10 ppb over the oil palm plantation) (Hewitt et al., 2010).

Halogen chemistry offers a mechanism for conversion of HO_2 to OH (Alicke et al., 1999; Heard and Pilling, 2003; Monks et al., 2005; Whalley et al., 2010). Assuming instantaneous photolysis of the HOBr product to yield OH, the reaction of HO_2 with BrO would require a BrO concentration above 4 ppb for BrO to be considered as a potential candidate for the missing species. This is $\sim$3 orders of magnitude higher than observed concentrations in the troposphere (Monks, 2005; Mahajan et al., 2009). We therefore reject halogens as a mechanism to convert HO_2 to OH.

The values of $k_{HO_2+X}[X]$ and $k_{RO_2+X}[X]$ determined here can be used to investigate the concentrations required for the missing species. At an upper limit of $k_{HO_2+X} = 1\times10^{-10}\,cm^3\,s^{-1}$, based on approximate gas kinetic limit for a bimolecular rate coefficient, we require a campaign average concentration for species X on the order of 800 ppt. This leads to $k_{RO_2+X} = 2.46\times10^{-12}\,cm^3\,s^{-1}$. For a lower rate coefficient of $k_{HO_2+X} = 1\times10^{-11}\,cm^{-3}\,s^{-1}$ we would require a concentration of 8 ppb for the unknown species, giving $k_{RO_2+X} = 2.46\times10^{-13}\,cm^3\,s^{-1}$.

It is possible that species X is a known species in the model, potentially an oxidation product of isoprene, with unknown chemistry responsible for the conversion of RO_2 to HO_2 and HO_2 to OH. The constraints placed on X enable us to investigate this possibility. At the gas kinetic upper limit for k_{HO_2+X} ($1\times10^{-10}\,cm^3\,s^{-1}$) there is a restricted list of species within the model that are at a high enough concentration in the model to convert HO_2 to OH fast enough to be considered as potential candidates for the species X. Table 4 lists those species which have high enough concentration in the model to enable fast enough conversion of RO_2 to HO_2 and HO_2 to OH using $k_{HO_2+X} = 1\times10^{-10}\,cm^3\,s^{-1}$, and show positive correlation with the model failure for OH (ratio of observed to modelled concentration). There are, however, no species within the model which fulfil the concentration criteria for the missing species for every data point exhibiting model failure.

OH generation from a reaction between HO_2 and carbonyl species such as glyoxal and hydroxyacetone have been proposed by da Silva (2011), involving the production and subsequent unimolecular decomposition of an α-hydroxyperoxy radical. Although we find that the modelled concentrations of hydroxyacetone (ACETOL in Table 4) are sufficient for it to be considered a candidate for X, the main fate of the α-hydroxyperoxy radicals formed on interaction of such carbonyl species with HO_2 at the temperatures encountered during OP3 is expected to be dissociation back to HO_2 and the carbonyl species. Introduction of a non-reversible reaction in the model between hydroxyacetone and HO_2 to produce $CH_3C(O)OOH$, HCHO and OH (the α-hydroxyperoxy radical decomposition products predicted by da Silva, 2011) with a rate coefficient of $k = 1\times10^{-10}\,cm^3\,s^{-1}$ and between hydroxyacetone and RO_2 to produce HO_2 with a rate coefficient of $k = 2.46\times10^{-12}\,cm^3\,s^{-1}$ did little to improve the model success (observed to modelled ratios for isoprene impacted points of $5.06^{+3.48}_{-4.20}$ and $1.16^{+0.30}_{-0.30}$ for OH and HO_2, respectively).

HCHO was also considered as a potential contender for the species X, and is known to form an adduct with HO_2 (Veyret et al., 1989; Burrows et al., 1989; Anglada and Domingo, 2005). However, since HCHO provides a photolytic source of HO_x, a model run including reactions of HCHO with RO_2 to produce HO_2 and with HO_2 to produce OH reduces the modelled HCHO concentration and thus the HO_x production from HCHO photolysis, and does not provide a solution.

Although a species "X" may help to reconcile modelled and observed OH it is unclear what the missing species could be.

5.5　ISOPOOH + OH → Epoxide + OH

Figures 5k–l and 6k–l show the effects of implementation of the isoprene oxidation scheme proposed by Paulot et al. (2009) in which the hydroxy-hydroperoxides derived from isoprene (ISOPOOH) react with OH to produce soluble

Table 4. Species present in the model in sufficient concentration to be potential candidates for the missing species in production of HO_x in the reactions $RO_2 + X \rightarrow HO_2$ and $HO_2 + X \rightarrow OH$ using $k_{HO2+X} = 1 \times 10^{-10}$ cm^3 s^{-1}. Linear fits to model success ($[HO_x]_{obs/mod}$ vs species) are given together with the corresponding r^2 value. Chemical names are as used in the MCM.

Species	Linear fit $[OH]_{obs/mod}$ vs. species (in cm^{-3})	r^2	Linear fit $[HO_2]_{obs/mod}$ vs. species (in cm^{-3})	r^2
CH_3CO_3H	$y = (0.890 \pm 0.105)x - (1.128 \pm 0.169)$	0.184	$y = (0.268 \pm 0.069)x - (0.451 \pm 0.109)$	0.007
$HOCH_2COOH$	$y = (0.832 \pm 0.098)x - (0.796 \pm 0.131)$	0.184	$y = (0.255 \pm 0.053)x - (0.359 \pm 0.070)$	0.017
CH_3COOH	$y = (0.832 \pm 0.099)x - (1.073 \pm 0.163)$	0.181	$y = (0.254 \pm 0.067)x - (0.440 \pm 0.107)$	0.007
$HOCH_2CO_3H$	$y = (0.915 \pm 0.109)x - (0.880 \pm 0.141)$	0.179	$y = (0.275 \pm 0.059)x - (0.380 \pm 0.075)$	0.016
ISOPBOOH	$y = (0.978 \pm 0.156)x - (1.907 \pm 0.380)$	0.173	$y = (0.312 \pm 0.152)x - (0.731 \pm 0.383)$	0.003
CH_3OH	$y = (0.616 \pm 0.081)x - (0.722 \pm 0.135)$	0.121	$y = (0.183 \pm 0.032)x + (0.281 \pm 0.057)$	0.033
ACETOL	$y = (0.733 \pm 0.099)x - (1.237 \pm 0.206)$	0.110	$y = (0.231 \pm 0.028)x - (0.467 \pm 0.054)$	0.149
CH_3OOH	$y = (2.068 \pm 0.285)x - (4.687 \pm 0.683)$	0.100	$y = (0.649 \pm 0.112)x + (1.556 \pm 0.292)$	0.028
$HOCH_2CHO$	$y = (0.892 \pm 0.124)x - (1.600 \pm 0.261)$	0.098	$y = (0.295 \pm 0.062)x - (0.640 \pm 0.128)$	0.017
C_5H_8	$y = (0.720 \pm 0.134)x - (1.536 \pm 0.384)$	0.084	$y = (0.201 \pm 0.085)x + (0.617 \pm 0.237)$	0.006
HMVKBOOH	$y = (0.873 \pm 0.171)x - (0.855 \pm 0.255)$	0.062	$y = (0.257 \pm 0.049)x + (0.417 \pm 0.081)$	0.076
MVK	$y = (0.731 \pm 0.153)x - (1.393 \pm 0.385)$	0.047	$y = (0.223 \pm 0.046)x + (0.575 \pm 0.119)$	0.056
C59OOH	$y = (1.243 \pm 0.289)x - (1.738 \pm 0.511)$	0.039	$y = (0.415 \pm 0.211)x - (0.737 \pm 0.404)$	0.003
MACR	$y = (0.709 \pm 0.166)x - (0.780 \pm 0.290)$	0.033	$y = (0.166 \pm 0.001)x - (0.235 \pm 0.001)$	<0.001
HCHO	$y = (1.006 \pm 0.191)x - (2.533 \pm 0.532)$	0.027	$y = (0.358 \pm 0.133)x - (1.011 \pm 0.363)$	0.002
H_2O_2	$y = (1.484 \pm 0.336)x - (3.989 \pm 0.962)$	0.014	$y = (0.530 \pm 0.101)x + (1.499 \pm 0.292)$	0.024
H_2O	$y = (1.958 \pm 0.448)x - (19.730 \pm 4.572)$	0.013	$y = (0.069 \pm 0.164)x - (7.029 \pm 1.677)$	0.010
PAN	$y = (0.831 \pm 0.196)x - (0.910 \pm 0.278)$	0.012	$y = (0.262 \pm 0.078)x - (0.404 \pm 0.111)$	0.004
C_3H_6	$y = (2.724 \pm 1.523)x - (3.549 \pm 2.130)$	<0.001	$y = (0.890 \pm 0.126)x - (1.262 \pm 0.174)$	0.082
CH_3COCH_3	$y = (0.607 \pm 0.001)x - (0.573 \pm 0.001)$	<0.001	$y = (0.184 \pm 0.024)x + (0.246 \pm 0.038)$	0.119

Table 5. Mechanism used to investigate the effects of OH regeneration in epoxide formation, as proposed by Paulot et al. (2009). Values for the rate coefficients of $OH + C_5H_8$, $ISOPO_2 + NO$ and $ISOPO_2 + NO_3$ were used as described in the MCM. The photolysis rate of ISOPOOH was used as adopted in GEOS-Chem.

Reaction	Rate coefficient/cm^3 s^{-1}	Reference
$ISOPO_2 + HO_2$ $\rightarrow$ 0.88 ISOPOOH + 0.12 OH + 0.047 MACR + 0.073 MVK + 0.12 HO_2 + 0.12 HCHO	7.40×10^{-13} exp$(700/T)$	Paulot et al. (2009)
$ISOPOOH + OH \rightarrow IEPOX + OH$	1.90×10^{-11} exp$(390/T)$	Paulot et al. (2009)
$ISOPOOH + OH$ $\rightarrow$ 0.7 ISOPOO + 0.3 HC5 + 0.3 OH	3.8×10^{-12} exp$(200/T)$	Paulot et al. (2009)
$IEPOX + OH \rightarrow IEPOXOO$	5.78×10^{-11} exp$(-400/T)$	Paulot et al. (2009)
$IEPOXOO + HO_2$ $\rightarrow$ 0.725 ACETOL + 0.275 $HOCH_2CHO$ + 0.275 GLYOX + 0.275 MGLYOX + 0.125 OH + 0.825 HO_2 + 0.2 CO_2 + 0.375 HCHO + 0.074 HCOOH + 0.251 CO	7.40×10^{-13} exp$(700/T)$	Paulot et al. (2009)

epoxide species and regenerate OH. Details of the reactions implemented in the model are given in Table 5. We use the reaction scheme as provided by Paulot et al. (2009) for implementation in the GEOS-CHEM global model, using the GEOS-CHEM photolysis reaction products of ISOPOOH and MCM chemistry for reactions of $ISOPO_2$ radicals with NO and NO_3. No reactions of $ISOPO_2$ radicals with any peroxy radical other than HO_2 have been included. An atmospheric lifetime for physical loss of IEPOX was set to approximately 24 h ($k_{loss} = 1 \times 10^{-5}$ s^{-1}), consistent with other species in the model (Sect. 3).

While the production of the epoxide species by reaction of OH with ISOPOOH is effectively OH neutral, the loss of OH in the initial $OH + C_5H_8$ step is not negated, and there is further loss of HO_x in the non-epoxide producing channel in $OH + ISOPOOH$, $OH + $ epoxide, and in the production of ISOPOOH from $HO_2 + ISOPO_2$. Figures 5k and 6k show little improvement in the model success for OH compared

Table 6. Reactions included in addition to the MCM to represent decomposition of β-ISOPO$_2$ radicals as proposed by da Silva et al. (2010).

Reaction	Rate coefficient/s^{-1}	Reference
ISOPBO$_2$ → MVK + HCHO + OH	$2.38 \times 10^{12} \exp(-21\,400/1.987T)$	da Silva et al. (2010)
ISOPDO$_2$ → MACR + HCHO + OH	$1.27 \times 10^{12} \exp(-21\,000/1.987T)$	da Silva et al. (2010)

to the base MCM run, and a statistically significant difference remains between the mean observed to modelled OH ratios for data points with isoprene above and below 15 ppt (Table 3). Wolfe et al. (2011) also found that additional OH sources were still required on inclusion of the epoxide scheme into the CAFE model during analysis of data from a ponderosa pine plantation during the BEARPEX campaign. Figure 7e shows the instantaneous OH budget for the same single point investigated for the base MCM run (Fig. 7a). There is little difference in the dominant chemistry for OH between the two simulations. Production of OH for both the MCM run and using the Paulot scheme is dominated by HO$_2$ + NO and O$_3$ photolysis, and loss reactions are dominated by OH + C$_5$H$_8$. The epoxide scheme shows an increased dominance of OH + HCHO, and shows considerable loss of OH through OH + epoxide. An increased physical loss of the epoxide to give an atmospheric lifetime of 1 h ($k_{loss} = 2.78 \times 10^{-4}$ s^{-1}) reduces the loss of OH through reaction with the epoxide, but the resulting change in the modelled OH does not significantly improve the model success.

Simulated concentrations of HO$_2$ are slightly increased using the epoxide scheme, as shown in Figs. 5l and 6l. For data points with isoprene above 15 ppt the mean observed to modelled HO$_2$ ratio is reduced from $1.18^{+0.30}_{-0.30}$ using the MCM to $0.96^{+0.24}_{-0.24}$ using the epoxide mechanism (with the ∼24 h lifetime for physical loss of IEPOX). While this increase in modelled HO$_2$ at isoprene concentrations above 15 ppt leads to similar model success for data points with isoprene above and below 15 ppt (Fig. 5l), diagnosis of the HO$_2$ budget (Fig. 7f) indicates that the difference arises owing to a difference in the rate of HO$_2$ + ISOPO$_2$ in the epoxide scheme recommended by Paulot et al. (2009) to that used in the MCM. At 298 K, the rate coefficient for HO$_2$ + ISOPO$_2$ in the epoxide scheme is 7.75×10^{-12} cm^3 s^{-1}, while the MCM uses 1.61×10^{-11} cm^3 s^{-1} due to differences in the way the rate coefficient has been predicted from measurements of rate coefficients of HO$_2$ with other RO$_2$ radicals.

5.6 Unimolecular decomposition in β-ISOPO$_2$ → OH

Density Functional Theory calculations by da Silva et al. (2010) suggest that β-ISOPO$_2$ radicals (ISOPBO$_2$ and ISOPDO$_2$ in the MCM) may experience a unimolecular thermal decomposition process involving an intramolecular H-shift, resulting in the production of OH, HCHO and either MVK (from ISOPBO$_2$) or MACR (from ISOPDO$_2$). We in-

clude these reactions as additional processes to the normal MCM chemistry, using the rate coefficients given in Table 6.

Figures 5m–n and 6m–n show the consequences of the decomposition process in ISOPBO$_2$ and ISOPDO$_2$ on the modelled OH and HO$_2$ for OP3. Little difference from the MCM base run is observed and significant differences in model success remain for both OH and HO$_2$ for data points with isoprene above and below 15 ppt. Although the unimolecular decomposition of β-ISOPO$_2$ radicals does provide a novel pathway for OH production, its effects on the modelled HO$_x$ are limited due to competing bimolecular reactions of the β-ISOPO$_2$ radicals with HO$_2$ and NO. Indeed, da Silva et al. do predict that the decomposition process is only likely to be influential in the marine boundary layer, where concentrations of both HO$_2$ and NO are low.

5.7 Unimolecular decomposition in glyoxal and carboxylic acid oxidation → OH

Further calculations by da Silva (2010a, b, 2011) have also proposed recycling of OH in glyoxal oxidation and in the oxidation of carboxylic acids. Glyoxal is an oxidation product of a number of anthropogenic and biogenic VOCs, including isoprene, while carboxylic acids are both emitted directly and produced by oxidation of other VOCs.

These OH recycling mechanisms involve unimolecular processes, occurring in competition with bimolecular reactions with HO$_2$ and NO (da Silva, 2010a, b). Such processes are unlikely to dominate at the NO and HO$_2$ concentrations encountered during OP3, similarly to the competition between unimolecular decomposition of β-ISOPO$_2$ radicals and reactions with HO$_2$ and NO described previously. Moreover, for the base MCM run loss of OH through reactions with glyoxal and carboxylic acids represents a small fraction of the total OH loss (0.23 % for glyoxal and 0.07 % for acetic acid, the dominant carboxylic acid in the model). Recycling of OH by these unimolecular processes, even if they were to dominate over the bimolecular reactions, would not provide sufficient increases to the modelled OH concentrations for OP3 to explain the model discrepancy.

5.8 Unimolecular decomposition in δ-ISOPO$_2$ → → OH + HO$_2$

Theoretical studies of ISOPO$_2$ radicals predict unimolecular processes which lead to the formation of both OH and HO$_2$ (Peeters et al., 2009; Peeters and Muller, 2010). One of the

Table 7. Mechanism used to model recycling of OH and HO_2 in isoprene photo-oxidation, as proposed by Peeters et al. (2009) and Peeters and Muller (2010). Rate coefficients for second order reactions are in cm^3 s^{-1}, those for first order reactions and photolysis reactions are in s^{-1}.

Reaction	Rate coefficient/cm^3 s^{-1} or s^{-1}	Reference
$C_5H_8 + OH \rightarrow ISOP1$	2.54×10^{-11} exp$(410/T) \times 0.5 \times 0.66$	Peeters et al. (2009)
$C_5H_8 + OH \rightarrow ISOP2$	2.54×10^{-11} exp$(410/T) \times 0.5 \times 0.66$	Peeters et al. (2009)
$C_5H_8 + OH \rightarrow ISOP3$	2.54×10^{-11} exp$(410/T) \times 0.5 \times 0.34$	Peeters et al. (2009)
$C_5H_8 + OH \rightarrow ISOP4$	2.54×10^{-11} exp$(410/T) \times 0.5 \times 0.34$	Peeters et al. (2009)
$ISOP1 \rightarrow ISOPEO_2$	3.1×10^{12} exp$(-7900/T) \times 9.8 \times 10^{-26}$ exp$(7900/T) \times [O_2]$	Peeters et al. (2009)
$ISOPEO_2 \rightarrow ISOP1$	3.1×10^{12} exp$(-7900/T)$	Peeters et al. (2009)
$ISOP1 \rightarrow ISOPBO_2$	3.7×10^{14} exp$(-9750/T) \times 4.0 \times 10^{-27}$ exp$(9570/T) \times [O_2]$	Peeters et al. (2009)
$ISOPBO_2 \rightarrow ISOP1$	3.7×10^{14} exp$(-9570/T)$	Peeters et al. (2009)
$ISOP2 \rightarrow ISOPBO_2$	4.2×10^{14} exp$(-9970/T) \times 3.57 \times 10^{-27}$ exp$(9970/T) \times [O_2]$	Peeters et al. (2009)
$ISOPBO_2 \rightarrow ISOP2$	4.2×10^{14} exp$(-9970/T)$	Peeters et al. (2009)
$ISOP2 \rightarrow ISOPAO_2$	7.8×10^{13} exp$(-8660/T) \times 1.79 \times 10^{-26}$ exp$(8660/T) \times [O_2]$	Peeters et al. (2009)
$ISOPAO_2 \rightarrow ISOP2$	7.8×10^{13} exp$(-8660/T)$	Peeters et al. (2009)
$ISOPBO_2 \rightarrow OH + HCHO + MVK$	4.81×10^{11} exp$(-9203/T)$	Muller and Peeters (2010)
$ISOPAO_2 \rightarrow HPALD1 + HO_2$	8.48×10^8 exp$(-5930/T)$	Muller and Peeters (2010)
$ISOP3 \rightarrow ISOPCO_2$	5.65×10^{12} exp$(-8410/T) \times 5.38 \times 10^{-26}$ exp$(8405/T) \times [O_2]$	Peeters et al. (2009)
$ISOPCO_2 \rightarrow ISOP3$	5.65×10^{12} exp$(-8410/T)$	Peeters et al. (2009)
$ISOP3 \rightarrow ISOPDO_2$	5.0×10^{14} exp$(-10\,120/T) \times 3.07 \times 10^{-27}$ exp$(10\,116/T) \times [O_2]$	Peeters et al. (2009)
$ISOPDO_2 \rightarrow ISOP3$	5.0×10^{14} exp$(-10\,120/T)$	Peeters et al. (2009)
$ISOP4 \rightarrow ISOPDO_2$	8.25×10^{14} exp$(-10\,220/T) \times 1.82 \times 10^{-27}$ exp$(10\,216/T) \times [O_2]$	Peeters et al. (2009)
$ISOP4 \rightarrow ISOPDO_2$	8.25×10^{14} exp$(-10\,220/T) \times 3.07 \times 10^{-27}$ exp$(10\,116/T) \times [O_2]$	Peeters et al. (2009)
$ISOP4 \rightarrow ISOPGO_2$	1.4×10^{14} exp$(-9110/T) \times 7.01 \times 10^{-27}$ exp$(9110/T) \times [O_2]$	Peeters et al. (2009)
$ISOPGO_2 \rightarrow ISOP4$	1.4×10^{14} exp$(-9110/T)$	Peeters et al. (2009)
$ISOPDO_2 \rightarrow OH + HCHO + MACR$	4.81×10^{11} exp$(-9203/T)$	Muller and Peeters (2010)
$ISOPGO_2 \rightarrow HPALD2 + HO_2$	8.48×10^8 exp$(-5930/T)$	Muller and Peeters (2010)
$HPALD1 \rightarrow PACALD1 + OH + HO_2$	4×10^{-4}	Peeters et al. (2009)
$HPALD2 \rightarrow PACALD2 + OH + HO_2$	4×10^{-4}	Peeters et al. (2009)
$PACALD1 \rightarrow HOCH_2CHO + CH_3CO_3 + OH$	1×10^{-3}	Peeters et al. (2009)
$PACALD2 \rightarrow ACETOL + CO + HO_2 + OH$	1×10^{-3}	Peeters et al. (2009)
$HPALD1 + OH \rightarrow PACALD1 + OH$	5.0×10^{-11}	Peeters et al. (2009)
$HPALD2 + OH \rightarrow PACALD2 + OH$	5.0×10^{-11}	Peeters et al. (2009)

key features of the scheme considered by Peeters et al. (2009) is the rapid equilibrium between the initial OH-isoprene addition products (ISOPOH) and their corresponding $ISOPO_2$ isomers formed on reaction with molecular oxygen. This results in the greatest reaction flux occurring through the fastest product forming pathway. The fastest product forming pathway is expected to occur through unimolecular $ISOPO_2$ rearrangements involving a 1,6-H-shift, resulting in production of HO_2 and unsaturated hydroxyperoxy-aldehydes (HPALDs). Peeters et al. (2009) propose that the HPALD species will photolyse rapidly during the day to produce OH, thereby increasing the expected yield of both OH and HO_2. In addition, minor channels to OH, HCHO and either MVK or MACR are expected to occur by 1,5-H-shifts in $ISOPO_2$ isomers, with total expected yields of approximately 1 for OH and 0.7 for HO_2.

Details of the mechanism suggested by Peeters et al. (2009) and Peeters and Muller (2010) are given in Table 7. Where differences exist in rate coefficients between the Peeters mechanism and those currently in the MCM we

use those predicted by Peeters et al. (2009) and Peeters and Muller (2010). Four additional $ISOPO_2$ isomers are incorporated in the Peeters mechanism that are not currently included in the MCM. Two of these, labelled here as $ISOPEO_2$ and $ISOPGO_2$, were approximated to behave in an identical fashion with respect to HO_2, RO_2 and NO as their MCM structural analogue $ISOPAO_2$. The other two additional $ISOPO_2$ isomers, labelled here as $ISOPFO_2$ and $ISOPHO_2$, are the HPALD producing isomers and we assume production of the corresponding HPALD isomer (HPALD1 and HPALD2 respectively) with 100 % yield.

Photolysis of HPALDs is predicted to be rapid during the day (j(HPALD) $\sim 3 \times 10^{-4}$ s^{-1} at noon) due to the combination of the unsaturated aldehyde moiety and the hydroperoxide functional group (Peeters et al., 2009; Peeters and Muller, 2010) and is expected to produce OH radicals in 100 % yield, thus providing an efficient mechanism for OH recycling in isoprene oxidation.

Table 8. Sensitivity of model output to key reaction rates in the Peeters mechansim. Mean ratios of observed to modelled OH and HO_2 are given for data points where isoprene concentrations are greater than 15 ppt. Mean ratios of observed to modelled OH and HO_2 for data points where isoprene concentrations were lower than 15 ppt were not significantly different to those given in Table 3 for the standard Peeters mechanism. The mechanism for the base Peeters model run is given in Table 7. P_D refers to the probability result of the Kolmorogov-Smirnov test and refers to the probability that the distribution functions of the ratios for data points with isoprene above and below 15 ppt are statistically identical. P_H refers to the probability result of the Kruskal-Wallis test and indicates the probability that the ratios for data points with isoprene concentrations above 15 ppt are independent of the isoprene concentration. Probability values less than 0.001 are listed as zero.

Model run	Mean $[OH]_{obs/mod}$, $C_5H_8 > 15$ ppt	P_D	P_H	Mean $[HO_2]_{obs/mod}$, $C_5H_8 > 15$ ppt	P_D	P_H
Base Peeters run	$1.50^{+1.12}_{-1.14}$	0.820	0.014	$0.46^{+0.18}_{-0.19}$	0	0
HPALD + OH → PACALD (no OH recycling)	$1.62^{+1.23}_{-1.22}$	0.884	0.029	$0.47^{+0.18}_{-0.19}$	0	0
PACALD2 + $h\nu$ → ACETOL + CO + OH (i.e. no HO_2)	$1.53^{+1.14}_{-1.16}$	0.820	0.017	$0.48^{+0.19}_{-0.19}$	0	0
PACALD1 + $h\nu$ → $HOCH_2CHO$ + CH_3CO3 + 2 OH and PACALD2 + $h\nu$ → ACETOL + CO + 2 OH (i.e. 2 OH and no HO_2)	$1.19^{+0.90}_{-0.86}$	0.006	0.002	$0.42^{+0.18}_{-0.18}$	0	0
$k/5$ for $ISOPO_2$ → HPALD + HO_2	$2.00^{+1.47}_{-1.52}$	0.035	0.028	$0.60^{+0.21}_{-0.22}$	0	0
$k/5$ for $ISOPO_2$ → HPALD + HO_2 and PACALD2 + $h\nu$ → ACETOL + CO + OH (i.e. no HO_2)	$2.02^{+1.48}_{-1.53}$	0.029	0.026	$0.63^{+0.22}_{-0.22}$	0	0
$k/5$ for $ISOPO_2$ → HPALD + HO_2 and PACALD2 + $h\nu$ → ACETOL + CO + OH (i.e. no HO_2) and HPALD + $h\nu$ → PACALD + OH (i.e. no HO_2)	$2.09^{+1.53}_{-1.59}$	0.016	0.023	$0.68^{+0.23}_{-0.23}$	0	0
$k/10$ for $ISOPO_2$ → HPALD + HO_2 and PACALD2 + $h\nu$ → ACETOL + CO + OH (i.e. no HO_2) and HPALD + $h\nu$ → PACALD + OH (i.e. no HO_2)	$2.40^{+1.75}_{-1.83}$	0	0.016	$0.76^{+0.24}_{-0.24}$	0	0
$k/10$ for $ISOPO_2$ → HPALD + HO_2 and PACALD2 + $h\nu$ → ACETOL + CO + OH (i.e. no HO_2) and HPALD + $h\nu$ → PACALD + OH (i.e. no HO_2) and $k/5$ for $ISOPBO_2$ → OH + HCHO + MVK and $k/5$ for $ISOPDO_2$ → OH + HCHO + MACR	$2.64^{+1.93}_{-2.03}$	0	0.011	$0.78^{+0.24}_{-0.24}$	0.001	0

The organic products of HPALD photolysis are expected to undergo a series of rapid unimolecular H-shifts and reactions with molecular oxygen to generate HO_2 and peroxy acid aldehydes (PACALDs). The PACALD species are also thought to be extremely photolabile (j(PACALD) $\sim 1 \times 10^{-3}$ s^{-1}), and further production of OH on PACALD photolysis has been proposed (Peeters et al., 2009; Peeters and Muller, 2010).

We consider the co-products of PACALD photolysis in analogy with photolysis of the structurally similar MCM species $HC4ACO_3H$ and $HC4CCO_3H$, which in addition to OH produce CH_3COCH_2OH (ACETOL), CO and HO_2 and $HOCH_2CHO$ and CH_3CO_3, respectively. Although the Peeters mechanism expects production of ketenes on photolysis of the PACALDs, further oxidation chemistry for such ketene species is, at the present, unavailable, and we use the MCM analogues at this point in the scheme in an attempt to provide a full isoprene degradation scheme. Sensitivity of the Peeters mechanism to the PACALD photolysis products is shown in Table 8. We also consider reactions of OH with HPALDs to occur in competition with photolysis, but the

proposed mechanisms are OH neutral for these reactions, and result in prompt formation of the PACALD species (Peeters et al., 2009; Peeters and Muller, 2010).

Figures 5o–p and 6o–p show the impact of the Peeters mechanism on the modelled HO_x for OP3. The modelled OH concentrations show a considerable improvement compared to the standard MCM base model run, with this scheme providing the greatest increase in the modelled OH by a viable mechanism observed thus far. Figure 7g shows the instantaneous OH budget for the single point used in Fig. 7a, indicating that much of the observed increase in OH results from HPALD and PACALD photolysis.

The probability distribution functions for the observed to modelled OH ratios for data points with isoprene above and below 15 ppt (Fig. 5o), and accompanying Kolmogorov-Smirnov test in Table 3, show that there is no statistically significant difference between the model success for OH for the two regimes using this mechanism. The observed to modelled ratio for OH does, however, show some small dependence on the isoprene concentration. Figure 6o shows that the observed to modelled ratio for OH is lower at high

isoprene concentrations than at low isoprene concentrations, and the Kruskal-Wallis test (Table 3) indicates a low probability ($P = 0.014$) that there is no difference in the ratio as a function of the isoprene concentration. However, the Peeters mechanism does provide a significant improvement in the model's ability to simulate the observed OH concentrations.

Figures 5p and 6p and Table 3 show the model results for HO_2, revealing that the HO_2 concentrations predicted by the Peeters scheme are significantly higher than the observed concentrations. Figure 7h shows the instantaneous HO_2 budget for the single point shown in Fig. 7b and reveals both an increased flux of HO_2 compared to the base MCM run (due to an increase in OH and therefore total HO_x) and significant production of HO_2 on both production and photolysis of the HPALDs. Photolysis of one of the PACALD isomers also produces HO_2 in our base simulation using the Peeters mechanism as a result of the use of MCM structural analogues for the PACALD photolysis products, contributing to the observed increase in HO_2. Sensitivity of the model to this is discussed below.

There are significant uncertainties in the calculated rate coefficients for the Peeters mechanism, with estimated uncertainties of a factor of $\sim$5 (Peeters et al., 2009; Peeters and Muller, 2010). The fate of the PACALD photolysis products is also a significant source of uncertainty in the model. We have investigated various combinations of reductions to key rate coefficients in the scheme and changes to HPALD and PACALD photolysis products. Table 8 lists the sensitivity analyses conducted and shows the mean observed to modelled ratios for OH and HO_2 and results of the Kolmogorov-Smirnov and Kruskal-Wallis tests for each of these model runs. We have been unable to find a scheme able to reproduce both the OH and HO_2 observations. Thus although the Peeters mechanism appears to remove the model bias in OH, it reappears in HO_2.

6 Impact of mechanistic changes

Figures 5 and 6 and Table 3 show the impact of the mechanistic changes on the mean observed to modelled ratios for OH and HO_2 for each scheme investigated. The base MCM run significantly underpredicts the observed OH concentrations. While improvements to the modelled OH concentration are possible through direct recycling of OH (Kubistin et al., 2008) and production from $HO_2 + ISOPO_2$ (Lelieveld et al., 2008; Butler et al., 2008; Kubistin et al., 2010), the yields of OH required from these mechanisms to rectify the model discrepancy are not compatible with available evidence (Hasson et al., 2004; Le Crane et al., 2006; Jenkin et al., 2007, 2008, 2010; Dillon and Crowley, 2008) and are unlikely to operate. Formation of an isoprene-derived epoxide species (Paulot et al., 2009), or production of OH from unimolecular

decomposition of β-$ISOPO_2$ radicals (da Silva et al., 2010) do little to improve the model discrepancy for OH.

Formation of OH by an unknown species responsible for conversion of RO_2 to HO_2 and HO_2 to OH remains a possibility, although the impact on RO_2 is difficult to assess due to the lack of aircraft observations of RO_2 during OP3, and has also been proposed as a potential mechanism to improve model success for the ground-based OP3 campaign (Whalley et al., 2011). Based on the model requirements for the unknown species to replicate the HO_x observations we do not expect the involvement of halogen chemistry since the concentrations of BrO required would exceed 4 ppb. Known species in the model that are potential candidates for involvement in these conversion reactions are limited to those shown in Table 4. Most of these are unmeasured and observations of their concentrations may offer some constraint on the system.

The possibility for production of large amounts of OH by a combination of reactions involving VOC oxidation products formed in small yields should not be rejected. Theoretical studies have indicated that OH may be produced by unimolecular processes in a number of different compounds (da Silva et al., 2010; da Silva, 2010a, b, 2011; Peeters et al., 2009; Chen et al., 2011) and the combined effects of a large number of as yet unreported such processes may provide significant improvements to the model success. The OH budget given in Fig. 7a for the base MCM run shows that while OH loss by any single species is dominated by isoprene, there are still a large number of reactions remaining for which concentrations of the species in question are unmeasured and reaction rates and products may be uncertain. Interactions between HO_2 and carbonyl compounds certainly warrant further attention with respect to their potential for producing OH radicals.

We find significant improvement to the model success for OH using the Peeters mechanism (Peeters et al., 2009). However, the Peeters mechanism leads to a significant model overestimation of HO_2, which may reflect the large uncertainties in the calculated rate coefficients and uncertainty in the fate of PACALD photolysis products. We have not been able to model observations of both OH and HO_2 with the results from any single model run.

This inability to simulate both OH and HO_2 simultaneously is not unique to the Peeters mechanism. We observe that mechanisms which can adequately describe the OH observations tend to overpredict the HO_2 concentrations. This indicates that there are outstanding problems in our understanding of HO_x chemistry in this region.

7   Conclusions

It is not obvious that further field studies will help to explain the model failure. However, observations of some of the new postulated species (epoxides, HPALDs etc.) may allow further progress to be made.

Further laboratory experiments are required to elucidate the mechanisms involved in the oxidation of isoprene. Such studies may provide a solution which enables reproduction of observations of both OH and HO_2 by the model. However, until this has been achieved, our results indicate that in order to obtain model to observation agreement for OH we require additional loss processes for HO_2. Any potential interference in the HO_2 measurements derived from alkene-based peroxy radicals, as discussed by Fuchs et al. (2011), will lead to a greater model discrepancy for HO_2 when agreement is achieved for OH, and the need for much greater additional loss processes for HO_2 than is indicated here.

The oxidation of isoprene in the atmosphere plays a significant role in understanding air quality and climate change. The changing emissions of isoprene in future climates due to increases in temperature and changing land use is one of the major driving forces for changes in atmospheric composition. This study emphasises that significant gaps exist in our knowledge of the chemistry of isoprene which lead to significant reductions in our confidence in simulations of the future composition of the atmosphere. None of the mechanistic suggestions available can reconcile both the OH and HO_2 observations.

References

Alicke, B., Hebestreit, K., Stutz, J., and Platt, U.: Iodine oxide in the marine boundary layer, Nature, 397, 572–573, 1999.

Anglada, J. M. and Domingo, V. M.: Mechanism for the Gas-Phase Reaction between Formaldehyde and Hydroperoxyl Radical. A Theoretical Study, J. Phys. Chem. A., 109, 10786–10794, 2005.

Archibald, A. T., Cooke, M. C., Utembe, S. R., Shallcross, D. E., Derwent, R. G., and Jenkin, M. E.: Impacts of mechanistic changes on HO_x formation and recycling in the oxidation of isoprene, Atmos. Chem. Phys., 10, 8097–8118, doi:10.5194/acp-10-8097-2010, 2010.

Archibald, A. T., Levine, J. G., Abraham, N. L., Cooke, M. C., Edwards, P. E., Heard, D. E., Jenkin, M. E., Pike, R. C.,

Monks, P., Shallcross, D. E., Teford, P. J., Whalley, L. K., and Pyle, J. A.: Impacts of HO_x regeneration and recycling in the oxidation of isoprene: Consequences for the composition of past, present and future atmospheres, Geophys. Res. Lett., 38, L05804, doi:10.1029/2010GL046520, 2011.

Bloss, W. J., Gravestock, T. J., Heard, D. E., Ingham, T., Johnson, G. P., and Lee, J. D.: Application of a compact all solid-state laser system to the in situ detection of atmospheric OH, HO_2, NO and IO by laser-induced fluorescence, J. Environ. Monit., 5, 21–28, 2003.

Brough, N., Reeves, C. E., Penkett, S. A., Stewart, D. J., Dewey, K., Kent, J., Barjat, H., Monks, P. S., Ziereis, H., Stock, P., Huntrieser, H., and Schlager, H.: Intercomparison of aircraft instruments on board the C-130 and Falcon 20 over southern Germany during EXPORT 2000, Atmos. Chem. Phys., 3, 2127–2138, doi:10.5194/acp-3-2127-2003, 2003.

Burrows, J. P., Moortgat, G. K., Tyndall, G. S., Cox, R. A., Jenkin, M. E., Hayman, G. D., and Veyret, B.: Kinetics and Mechanism of the Photooxidation of Formaldehyde. 2. Molecular Modulation Studies, J. Phys. Chem., 93, 2375–2382, 1989.

Butler, T. M., Taraborrelli, D., Brühl, C., Fischer, H., Harder, H., Martinez, M., Williams, J., Lawrence, M. G., and Lelieveld, J.: Improved simulation of isoprene oxidation chemistry with the ECHAM5/MESSy chemistry-climate model: lessons from the GABRIEL airborne field campaign, Atmos. Chem. Phys., 8, 4529–4546, doi:10.5194/acp-8-4529-2008, 2008.

Capes, G., Murphy, J. G., Reeves, C. E., McQuaid, J. B., Hamilton, J. F., Hopkins, J. R., Crosier, J., Williams, P. I., and Coe, H.: Secondary organic aerosol from biogenic VOCs over West Africa during AMMA, Atmos. Chem. Phys., 9, 3841–3850, doi:10.5194/acp-9-3841-2009, 2009.

Carslaw, N., Creasey, D. J., Harrison, D., Heard, D. E., Hunter, M. C., Jacobs, P. J., Jenkin, M. E., Lee, J. D., Lewis, A. C., Pilling, M. J., Saunders, S. M., and Seakins, P. W.: OH and HO_2 radical chemistry in a forested region of north-western Greece, Atmos. Environ., 35, 4725–4737, 2001.

Chen, D., Jin, H., Wang, Z., Zhang, L., and Qi, F.: Unimolecular Decomposition of Ethyl Hydroperoxide: Ab Initio/Rice-Ramsperger-Kassel-Marcus Theoretical Prediction of Rate Constants, J. Phys. Chem. A., 115(5), 602–611, 2011.

Commane, R., Floquet, C. F. A., Ingham, T., Stone, D., Evans, M. J., and Heard, D. E.: Observations of OH and HO2 radicals over West Africa, Atmos. Chem. Phys., 10, 8783–8801, doi:10.5194/acp-10-8783-2010, 2010.

da Silva, G.: Hydroxyl radical regeneration in the photochemical oxidation of glyoxal: kinetics and mechanism of the HC(O)CO + O_2 reaction, Phys. Chem. Chem. Phys., 12, 6698–6705, 2010a.

da Silva, G.: Oxidation of Carboxylic Acids Regenerates Hydroxyl Radicals in the Unpolluted and Nighttime Troposphere, J. Phys. Chem. A., 114, 6861–6869, 2010b.

da Silva, G.: Kinetics and Mechanism of the Glyoxal + HO_2 Reaction: Conversion of HO_2 to OH by Carbonyls, J. Phys. Chem. A., 115, 291–297, 2011.

da Silva, G., Graham, C., and Wang, Z. F.: Unimolecular β-Hydroperoxy Radical Decomposition with OH Recycling in the Photochemical Oxidation of Isoprene, Environ. Sci. Technol., 44, 250–256, 2010.

Dillon, T. J. and Crowley, J. N.: Direct detection of OH formation in the reactions of HO_2 with $CH_3C(O)O_2$ and other sub-

stituted peroxy radicals, Atmos. Chem. Phys., 8, 4877–4889, doi:10.5194/acp-8-4877-2008, 2008.

Edwards, G. D. and Monks, P. S.: Performance of a single-monochromator diode array spectroradiometer for the determination of actinic flux and atmospheric photolysis frequencies, J. Geophys. Res., 108(D16), 8546, doi:10.1029/2002JD002844, 2003.

Edwards, P. M., Whalley, L. K., Furneaux, K. L., Stone, D., Goddard, A., Ingham, T., Hopkins, J., Jones, C., Lee, J. D.,Lewis, A. C., Moller, S., Robinson, N., Evans, M. J., and Heard, D. E.: OH reactivity in a South East Asian Tropical rainforest, Atmos. Chem. Phys. Discuss., in preparation, 2011.

Ehhalt, D. H. and Rohrer, F.: The tropospheric cycle of H_2: a critical review, Tellus, 61B, 500–535, 2009.

Emmerson, K. M. and Evans, M. J.: Comparison of tropospheric gas-phase chemistry schemes for use within global models, Atmos. Chem. Phys., 9, 1831–1845, doi:10.5194/acp-9-1831-2009, 2009.

Fuchs, H., Bohn, B., Hofzumahaus, A., Holland, F., Lu, K. D., Nehr, S., Rohrer, F., and Wahner, A.: Detection of HO2 by laser-induced fluorescence: calibration and interferences from RO2 radicals, Atmos. Meas. Tech., 4, 1209–1225, doi:10.5194/amt-4-1209-2011, 2011.

Gerbig, C., Schmitgen, S., Kley, D., Volz-Thomas, A., Dewey, K., and Haaks, D.: An improved fast-response vacuum UV resonance fluorescence CO instrument, J. Geophys. Res. Atmos., 104, 1699–1704, 1999.

GLOBALVIEW-CH4, 2009: Cooperative Atmospheric Data Integration Project – Methane. CD-ROM, NOAA ESRL, Boulder, Colorado, also available on Internet via anonymous FTP to ftp://ftp.cmdl.noaa.gov, path: ccg/CH4/GLOBALVIEW, 2009, access: 26 January 2011.

Hard, T. M., O'Brien, R. J., Chan, C. Y., and Mehrabzadeh, A. A.: Tropospheric Free-Radical Determination by FAGE, Environ. Sci. Technol., 18, 768–777, 1984.

Hasson, A. S., Tyndall, G. S., and Orlando, J. J.: A product yield study of the reaction of HO_2 radicals with ethyl peroxy ($C_2H_5O_2$), acetyl peroxy ($CH_3C(O)O_2$), and acetonyl peroxy ($CH_3C(O)CH_2O_2$) radicals, J. Phys. Chem. A, 108, 5979–5989, 2004.

Heard, D. E. and Pilling, M. J.: Measurement of OH and HO_2 in the troposphere, Chem. Reviews, 103, 5163–5198, 2003.

Hewitt, C. N., Lee, J. D., MacKenzie, A. R., Barkley, M. P., Carslaw, N., Carver, G. D., Chappell, N. A., Coe, H., Collier, C., Commane, R., Davies, F., Davison, B., DiCarlo, P., Di Marco, C. F., Dorsey, J. R., Edwards, P. M., Evans, M. J., Fowler, D., Furneaux, K. L., Gallagher, M., Guenther, A., Heard, D. E., Helfter, C., Hopkins, J., Ingham, T., Irwin, M., Jones, C., Karunaharan, A., Langford, B., Lewis, A. C., Lim, S. F., MacDonald, S. M., Mahajan, A. S., Malpass, S., McFiggans, G., Mills, G., Misztal, P., Moller, S., Monks, P. S., Nemitz, E., Nicolas-Perea, V., Oetjen, H., Oram, D. E., Palmer, P. I., Phillips, G. J., Pike, R., Plane, J. M. C., Pugh, T., Pyle, J. A., Reeves, C. E., Robinson, N. H., Stewart, D., Stone, D., Whalley, L. K., and Yin, X.: Overview: oxidant and particle photochemical processes above a south-east Asian tropical rainforest (the OP3 project): introduction, rationale, location characteristics and tools, Atmos. Chem. Phys., 10, 169–199, doi:10.5194/acp-10-169-2010, 2010.

Hofzumahaus, A., Rohrer, F., Lu, K., Bohn, B., Brauers, T., Chang, C. C., Fuchs, H., Holland, F., Kita, K., Kondo, Y., Li, X., Lou, S., Shao, M., Zeng, L., Wahner, A., and Zhang, Y.: Amplified trace gas removal in the troposphere, Science, 324, 1702–1704, 2009.

Hopkins, J. R., Lewis, A. C., and Read, K. A.: A two-column method for long-term monitoring of non-methane hydrocarbons (NMHCs) and oxygenated volatile organic compounds (oVOCs), J. Environ. Monit., 5, 8–13, 2003.

Hopkins, J. R., Evans, M. J., Lee, J. D., Lewis, A. C., H Marsham, J., McQuaid, J. B., Parker, D. J., Stewart, D. J., Reeves, C. E., and Purvis, R. M.: Direct estimates of emissions from the megacity of Lagos, Atmos. Chem. Phys., 9, 8471–8477, doi:10.5194/acp-9-8471-2009, 2009.

Jaegle, L., Jacob, D. J., Brune, W. H., Faloona, I., Tan, D., Heikes, B. G., Kondo, Y., Sachse, G. W., Anderson, B., Gregory, G. L., Singh, H. B., Pueschel, R., Ferry, G., Blake, D. R., and Shetter, R. E.: Photochemistry of HO_X in the uppoer troposphere at northern midlatitudes, J. Geophys. Res., 105(D3), 3877–3892, 2000.

Jenkin, M. E., Saunders, S. M., Wagner, V., and Pilling, M. J.: Protocol for the development of the Master Chemical Mechanism, MCM v3 (Part B): tropospheric degradation of aromatic volatile organic compounds, Atmos. Chem. Phys., 3, 181–193, doi:10.5194/acp-3-181-2003, 2003.

Jenkin, M. E., Hurley, M. D., and Wallington, T. J.: Investigation of the radical product channel of the $CH_3C(O)O_2+HO_2$ reaction in the gas phase, Phys. Chem. Chem. Phys., 9, 3149–3162, 2007.

Jenkin, M. E., Hurley, M. D., and Wallington, T. J.: Investigation of the radical product channel of the $CH_3C(O)CH_2O_2+HO_2$ reaction in the gas phase, Phys. Chem. Chem. Phys., 10, 4274–4280, 2008.

Jenkin, M. E., Hurley, M. D., and Wallington, T. J.: Investigation of the Radical Product Channel of the $CH_3OCH_2O_2 + HO_2$ Reaction in the Gas Phase, J. Phys. Chem. A., 114, 408–416, 2010.

Jones, C. E., Hopkins, J. R., and Lewis, A. C.: In situ measurements of isoprene and monoterpenes within a South-East Asian tropical rainforest, Atmos. Chem. Phys. Discuss., 11, 1189–1218, doi:10.5194/acpd-11-1189-2011, 2011.

Kolmorogov, A.: Sulla determinazione empirica di una legge di distribuzione, G. Inst. Ital. Attuari, 4, 83, 1933.

Kruskal, W. H. and Wallis, W. A.: Use of ranks in one-criterion variance analysis, J. Am. Stat. Assoc., 47(260), 583–621, 1952.

Kubistin, D., Harder, H., Martinez, M., Rudolf, M., Sander, R., Bozem, H., Eerdekens, G., Fischer, H., Gurk, C., Klpfel, T., Knigstedt, R., Parchatka, U., Schiller, C. L., Stickler, A., Taraborrelli, D., Williams, J., and Lelieveld, J.: Hydroxyl radicals in the tropical troposphere over the Suriname rainforest: comparison of measurements with the box model MECCA, Atmos. Chem. Phys., 10, 9705–9728, doi:10.5194/acp-10-9705-2010, 2010.

Le Crane, J. P., Rayez, M. T., Rayez, J. C., and Villenave, E.: A reinvestigation of the kinetics and the mechanism of the $CH_3C(O)O_2+HO_2$ reaction using both experimental and theoretical approaches, Phys. Chem. Chem. Phys., 8, 2163–2171, 2006.

Lelieveld, J., Butler, T. M., Crowley, J. N., Dillon, T. J., Fischer, H., Ganzeveld, L., Harder, H., Lawrence, M. G., Martinez, M., Taraborrelli, D., and Williams, J.: Atmospheric oxidation capacity sustained by a tropical forest, Nature, 452, 737–740, 2008.

Mahajan, A. S., Oetjen, H., Saiz-Lopez, A., Lee, J. D., McFig-

gans, G. B., and Plane, J. M. C.: Reactive iodine species in a semi-polluted environment, Geophys. Res. Lett., 36, L16803, doi:10.1029/2009GL038018, 2009.

Mao, J., Ren, X., Brune, W. H., Olson, J. R., Crawford, J. H., Fried, A., Huey, L. G., Cohen, R. C., Heikes, B., Singh, H. B., Blake, D. R., Sachse, G. W., Diskin, G. S., Hall, S. R., and Shetter, R. E.: Airborne measurement of OH reactivity during INTEX-B, Atmos. Chem. Phys., 9, 163–173, doi:10.5194/acp-9-163-2009, 2009.

Martinez, M., Harder, H., Kubistin, D., Rudolf, M., Bozem, H., Eerdekens, G., Fischer, H., Klüpfel, T., Gurk, C., Königstedt, R., Parchatka, U., Schiller, C. L., Stickler, A., Williams, J., and Lelieveld, J.: Hydroxyl radicals in the tropical troposphere over the Suriname rainforest: airborne measurements, Atmos. Chem. Phys., 10, 3759–3773, doi:10.5194/acp-10-3759-2010, 2010.

Monks, P. S.: Gas-phase radical chemistry in the troposphere, Chem. Soc. Rev., 34(5), 376–395, 2005.

Murphy, J. G., Oram, D. E., and Reeves, C. E.: Measurements of volatile organic compounds over West Africa, Atmos. Chem. Phys., 10, 5281–5294, doi:10.5194/acp-10-5281-2010, 2010.

Nguyen, T. L., Vereecken, L., and Peeters, J.: HO_x Regeneration in the Oxidation of Isoprene III: Theoretical Study of the key Isomerisation of the Z-δ-hydroxy-peroxy Isoprene Radicals, Chem. Phys. Chem., 11, 3996–4001, 2010

Novelli, P. C., Lang, P. M., Masarie, K. A., Hurst, D. F., Myers, R., and Elkins, J. W.: Molecular hydrogen in the troposphere: Global distribution and budget, J. Geophys. Res., 104(D23), 30427–30444, 1999.

Olson, J. R., Crawford, J. H., Chen, G., Fried, A., Evans, M. J., Jordan, C. E., Sandholm, S. T., Davis, D. D., Anderson, B. E., Avery, M. A., Barrick, J. D., Blake, D. R., Brune, W. H., Eisele, F. L., Flocke, F., Harder, H., Jacob, D. J., Kondo, Y., Lefer, B. L., Martinez, M., Mauldin, R. L., Sachse, G. W., Shetter, R. E., Singh, H. N., Talbot, R. W., and Tan, D.: Testing fast photochemical theory during TRACE-P based on measurements of OH, HO_2 and CH_2O, J. Geophys. Res., 109, D15S10, doi:10.1029/2003JD004278, 2004.

Olson, J. R., Crawford, J. H., Chen, G., Brune, W. H., Faloona, I. C., Tan, D., Harder, H., and Martinez, M.: A reevaluation of airborne HO_x observations from NASA field campaigns, J. Geophys. Res., 111, D10301, doi:10.1029/2005JD006617, 2006.

Paulot, F., Crounse, J. D., Kjaergaard, H. G., Kurten, A., St. Clair, J. M., Seinfeld, J. H., and Wennberg, P. O.: Unexpected Epoxide Formation in the Gas-Phase Photooxidation of Isoprene, Science, 325, 730–733, 2009.

Peeters, J. and Muller, J.-F.: HO_x radical regeneration in isoprene oxidation via peroxy radical isomerisations. II: experimental evidence and global impact, Phys. Chem. Chem. Phys., 12, 14227–14235, 2010.

Peeters, J., Nguyen, T. L., and Vereecken, L.: HO_x radical regeneration in the oxidation of isoprene, Phys. Chem. Chem. Phys., 11(28), 5935–5939, 2009.

Pugh, T. A. M., MacKenzie, A. R., Hewitt, C. N., Langford, B., Edwards, P. M., Furneaux, K. L., Heard, D. E., Hopkins, J. R., Jones, C. E., Karunaharan, A., Lee, J., Mills, G., Misztal, P., Moller, S., Monks, P. S., and Whalley, L. K.: Simulating atmospheric composition over a South-East Asian tropical rainforest: performance of a chemistry box model, Atmos. Chem. Phys., 10, 279–298, doi:10.5194/acp-10-279-2010, 2010.

Ren, X., Harder, H., Martinez, M., Faloona, I. C., Tan, D., Lesher, R. L., Di Carlo, P., Simpas, J. B., and Brune, W. H.: Interference Testing for Atmospheric HO_x Measurements by Laser-induced Fluorescence, J. Atmos. Chem., 47, 169–190, 2004.

Ren, R., Olson, J. R., Crawford, J. H., Brune, W. H., Mao, J., Long, R. B., Chen, Z., Chen, G., Avery, M. A., Sachse, G. W., Barrick, J. D., Diskin, G. S., Huey, L. G., Fried, A., Cohen, R. C., Heikes, B., Wennberg, P. O., Singh, H. B., Blake, D. R., and Shetter, R. E.: HO_x chemistry during INTEX-A 2004: Observation, model calculation, and comparison with previous studies, J. Geophys. Res., 113, D05310, doi:10.1029/2007JD009166, 2008.

Saunders, S. M., Jenkin, M. E., Derwent, R. G., and Pilling, M. J.: Protocol for the development of the Master Chemical Mechanism, MCM v3 (Part A): tropospheric degradation of non-aromatic volatile organic compounds, Atmos. Chem. Phys., 3, 161–180, doi:10.5194/acp-3-161-2003, 2003.

Smirnov, N. V.: Tables for estimating the goodness of fit of empirical distributions, Ann. Math. Stat., 19, 279, 1948.

Stavrakou, T., Peeters, J., and Müller, J.-F.: Improved global modelling of HO_x recycling in isoprene oxidation: evaluation against the GABRIEL and INTEX-A aircraft campaign measurements, Atmos. Chem. Phys., 10, 9863–9878, doi:10.5194/acp-10-9863-2010, 2010.

Stephens, M. A.: EDF Statistics for Goodnes of Fit and Some Comparisons, J. Am. Soc. Stat. Assoc., 69(347), 730–737, 1974.

Stewart, D. J., Taylor, C. M., Reeves, C. E., and McQuaid, J. B.: Biogenic nitrogen oxide emissions from soils: impact on NO_x and ozone over west Africa during AMMA (African Monsoon Multidisciplinary Analysis): observational study, Atmos. Chem. Phys., 8, 2285–2297, doi:10.5194/acp-8-2285-2008, 2008.

Stone, D., Evans, M. J., Commane, R., Ingham, T., Floquet, C. F. A., McQuaid, J. B., Brookes, D. M., Monks, P. S., Purvis, R., Hamilton, J. F., Hopkins, J., Lee, J., Lewis, A. C., Stewart, D., Murphy, J. G., Mills, G., Oram, D., Reeves, C. E., and Heard, D. E.: HO_x observations over West Africa during AMMA: impact of isoprene and NO_x, Atmos. Chem. Phys., 10, 9415–9429, doi:10.5194/acp-10-9415-2010, 2010.

Tan, D., Faloona, I., Simpas, J. B., Brune, W., Olson, J., Crawford, J., Avery, M., Sachse, G., Vay, S., Sandholm, S., Guan, H. W., Vaughn, T., Mastromarino, J., Heikes, B., Snow, J., Podolske, J., and Singh, H.: OH and HO_2 in the tropical Pacific: Results from PEM-Tropics B, J. Geophys. Res., 106, 32667–32681, 2001.

Thornton, J. A., Wooldridge, P. J., Cohen, R. C., Martinez, M., Harder, H., Brune, W. H., Williams, E. J., Roberts, J. M., Fehsenfeld, F. C., Hall, S. R., Shetter, R. E., Wert, B. P., and Fried, A.: Ozone production rates as a function of NOx abundances and HO_x production rates in the Nashville urban plume, J. Geophys. Res., 107, D124146, doi:10.1029/2001JD000932, 2002.

Veyret, B., Lesclaux, R., Rayez, M.-T., Rayez, J.-C., Cox, R. A., and Moortgat, G. K.: Kinetics and Mechanism of the Photooxidation of Formaldehyde. 1. Flash Photolysis Study, J. Phys. Chem., 93, 2368–2374, 1989.

Whalley, L. K., Furneaux, K. L., Goddard, A., Lee, J. D., Mahajan, A., Oetjen, H., Read, K. A., Kaaden, N., Carpenter, L. J., Lewis, A. C., Plane, J. M. C., Saltzman, E. S., Wiedensohler, A., and Heard, D. E.: The chemistry of OH and HO_2 radicals in the boundary layer over the tropical Atlantic Ocean, Atmos. Chem. Phys., 10, 1555–1576, doi:10.5194/acp-10-1555-2010, 2010.

Whalley, L. K., Edwards, P. M., Furneaux, K. L., Goddard, A.,

Ingham, T., Evans, M. J., Stone, D., Hopkins, J. R., Jones, C. E., Karunaharan, A., Lee, J. D., Lewis, A. C., Monks, P. S., Moller, S. J., and Heard, D. E.: Quantifying the magnitude of a missing hydroxyl radical source in a tropical rainforest, Atmos. Chem. Phys. Discuss., 11, 5785–5809, doi:10.5194/acpd-11-5785-2011, 2011.

Wolfe, G. M., Thornton, J. A., Bouvier-Brown, N. C., Goldstein, A. H., Park, J.-H., McKay, M., Matross, D. M., Mao, J., Brune, W. H., LaFranchi, B. W., Browne, E. C., Min, K.-E., Wooldridge, P. J., Cohen, R. C., Crounse, J. D., Faloona, I. C., Gilman, J. B., Kuster, W. C., de Gouw, J. A., Huisman, A., and Keutsch, F. N.: The Chemistry of Atmosphere-Forest Exchange (CAFE) Model – Part 2: Application to BEARPEX-2007 observations, Atmos. Chem. Phys., 11, 1269–1294, doi:10.5194/acp-11-1269-2011, 2011.